Simulation and Analysis of High Performance Parallel Resonant Converter for LED Driver

This thesis is submitted in the partial fulfilment of the requirements of the degree

MASTER IN CONTROL SYSTEM ENGINEERING

Submitted by

Nahid Anowar

Examination Roll Number: **M4CTL23007**

Registration Number: 160196 of 2021-22

Under the Guidance of

Dr. Debashis Chatterjee

Department of Electrical Engineering

Faculty of Engineering and Technology

JADAVPUR UNIVERSITY

KOLKATA–700032

August, 2023

Faculty of Engineering and Technology

JADAVPUR UNIVERSITY

Kolkata-700032

Certificate of Recommendation

This is to certify that **Mr. Nahid Anowar (0020110804004)** has completed his dissertation entitled, "**Simulation and Analysis of High Performance Parallel Resonant Converter for LED Driver**", under the direct supervision and guidance of **Dr. Debashis Chatterjee**, Department of Electrical Engineering, Jadavpur University. We are satisfied with his work, which is being presented for the partial fulfilment of the degree of **Master in Control System Engineering** of Jadavpur University, Kolkata-700032.

.....

Dr. Debashis Chatterjee

Professor,
Electrical Engineering Department
Jadavpur University, Kolkata-700032

.....

Prof. Biswanath Roy

Head of the Department,
Electrical Engineering Department,
Jadavpur University, Kolkata-700032

.....

Prof. Saswati Majumdar

Dean,
Faculty of Engineering & Technology
Jadavpur University, Kolkata-700032

Faculty of Engineering and Technology

JADAVPUR UNIVERSITY

Kolkata-700032

Certificate of Approval

The foregoing thesis entitled "**Simulation and Analysis of High Performance Parallel Resonant Converter for LED Driver**" is hereby approved as a creditable study of an Engineering subject carried out and presented in a manner satisfactory to warrant its acceptance as a pre-requisite to the degree of Master in Control System Engineering for which it has been submitted. It is understood that, by this approval the undersigned does not necessarily endorse or approve any statement made, opinion expressed, or conclusion therein but approve this thesis only for the purpose for which it is submitted.

Final Examination for Evaluation of the Thesis

……

……

……

Signature of the Examiners

Declaration of Originality

I hereby declare that this thesis contains a literature survey and original research work by the undersigned candidate, as part of his Master in Control System engineering curriculum. All information in this document has been obtained and presented in accordance with academic rules and ethical conduct. I also declare that, as required by these rules and conduct, I have fully cited and referenced all material and results that are not original to this work.

Name: Nahid Anowar

Examination Roll No.: M4CTL23007

Thesis Title: Simulation and Analysis of High Performance Parallel Resonant Converter for LED Driver

Signature with Date:

ACKNOWLEDGEMENT

I sincerely thank my supervisor, Prof. Dr. Debashis Chatterjee, Department of Electrical Engineering, Jadavpur University, Kolkata, for his invaluable guidance, suggestions, encouragement, and constant support throughout my thesis work, which helped me in successfully completing it. It was a great honour for me to pursue my research under his supervision.

I would also like to thank all my classmates Ujjwal Eman and Rajeev Ranjan Raj for their continuous help and support without which this would not have been possible.

I would like to express my gratitude towards all the staffs of control systems laboratory for providing constant encouragement throughout my thesis work.

Last but not the least, I extend my words of gratitude to my parents, Mr. Khadimul Islam and Mrs. Sabina Yeasmin, also my brother Wahid for their endless love support to guide me through every thick and thin of life.

Nahid Anowar

Jadavpur University,

Kolkata – 700032

ABSTRACT

Resonant converters have been an active area of research in power electronics field due to variety of topologies, diverse, peculiar and useful characteristics, and, wide applicability for voltage regulator modules, fluorescent lamps ballasts, power factor correction, capacitor charging, induction heating, welding, inductive power transfer, high-voltage power supply etc., due to soft switching, high frequency operation, high efficiency, and small size. While the majority of the previous work on resonant converters has been directed towards developing methods of analysis and control techniques for the mentioned applications, very little has been done to explore their suitability for application as a constant-current power supply, which is either inherently required or can be advantageously applied in electric arc welding, laser diode drivers, magnet power supplies, capacitor charging, illumination systems, battery charging, electrochemical processes etc..

The ever-increasing demand for energy-efficient lighting solutions has spurred significant advancements in LED technology and associated driver circuitry. This thesis presents a comprehensive investigation into the design, simulation, and analysis of a High-Performance Parallel Resonant Converter (HPPRC) tailored for LED driver applications. The primary focus lies in enhancing the efficiency, reliability, and overall performance of the driver circuit, thereby contributing to the broader goal of sustainable and energy-conservative illumination systems.

The research begins with an in-depth exploration of the theoretical underpinnings of parallel resonant converters and their applicability to LED driving. A systematic review of existing converter topologies, control strategies, and optimization techniques establishes the foundation for the subsequent stages of the study. Leveraging this theoretical framework, a novel HPPRC architecture is proposed, characterized by its ability to deliver improved power conversion efficiency while maintaining robust performance characteristics.

In pursuit of practical implementation, the thesis employs advanced simulation tools to model and analyse the designed HPPRC under various operating conditions and loading scenarios. The simulation results provide valuable insights into the converter's transient responses, steady-

state behaviours, and energy transfer dynamics. In addition, comprehensive sensitivity analyses are conducted to assess the impact of component variations, offering a deeper understanding of the converter's tolerance to real-world manufacturing variations and parameter uncertainties.

Furthermore, this research delves into control strategies tailored for the HPPRC, aiming to achieve optimal performance across the entire operating range. Both traditional control techniques and modern control algorithms are investigated, and their effectiveness in regulating key converter parameters is evaluated. The comparative study facilitates the identification of the most suitable control approach, thereby contributing to the HPPRC's reliability and adaptability in diverse lighting environments.

Through rigorous experimentation and validation, this thesis contributes a holistic understanding of the proposed HPPRC's capabilities and limitations. The results substantiate its potential to serve as a high-performance driver circuit for LEDs, demonstrating enhanced efficiency, reduced losses, and improved transient response compared to conventional solutions. The findings also highlight the converter's capacity to operate reliably under challenging conditions, making it a promising candidate for real-world LED lighting applications.

In conclusion, this research bridges the gap between theoretical concepts and practical implementations, presenting a meticulously examined High-Performance Parallel Resonant Converter tailored for LED driver applications. By offering novel insights into design, simulation, and control strategies, this work contributes to the advancement of energy-efficient lighting systems, aligning with contemporary sustainability goals and technological advancements.

CONTENTS

List Of Abbreviation

LED	Light-emitting diode
HPPRC	High-Performance Parallel Resonant Converter
PI	Proportional-Integral
MPC	Model Predictive Control
LLC	Inductor-Inductor-Capacitor
SRC	Silicon Controlled Rectifier
ZVS	Zero-Voltage-Switching
PRC	Parallel Resonant Converters
PWM	Pulse Width Modulation
PFC	Power Factor Correction
ZCS	Zero Current Switching
EMI	Electromagnetic interference
FHA	First Harmonic Approximation

List Of Figures

List Of Tables

Chapter 1

Introduction

1.1 History and Background

1.1.1 Evolution of LED Lighting Technology

The evolution of lighting technology has witnessed significant milestones, with Light Emitting Diodes (LEDs) emerging as a transformative solution. LEDs, initially developed as indicator lights, have rapidly evolved into versatile light sources owing to their high efficiency, longer lifespan, and low energy consumption. The shift towards energy-efficient lighting gained momentum as environmental concerns and the need for sustainable energy consumption grew more pronounced. This led to the exploration of novel lighting systems that aligned with the principles of energy conservation and reduced greenhouse gas emissions.

The early applications of LEDs were limited to low-power indicators and display units due to constraints in materials and fabrication techniques. However, advancements in semiconductor materials, epitaxial growth processes, and chip packaging technologies spurred the development of high-brightness LEDs capable of emitting light across the visible spectrum. This breakthrough expanded the application horizon of LEDs to general lighting, automotive lighting, and display backlighting.

1.1.2 LED Driver Circuitry and Power Conversion

Integral to the success of LEDs as illumination sources is the efficient conversion of electrical power into usable light. LED driver circuits play a pivotal role in ensuring optimal performance, maintaining appropriate current levels, and mitigating issues like color shift and flickering. The development of LED driver technologies progressed alongside the advancements in LED technology, ultimately shaping the landscape of modern lighting systems.

Early LED driver designs often utilized linear regulators, which, while simple, suffered from poor efficiency, limiting their suitability for high-power applications. The need for more efficient power conversion led to the exploration of switch-mode power supplies, including buck, boost, and buck-boost converters. These topologies offered improved efficiency by operating in a regulated switching mode, where power losses were substantially reduced compared to linear regulators.

1.1.3 Research Focus and Rationale

In the quest for even higher efficiency and performance, resonant power conversion topologies garnered attention. Resonant converters, characterized by their ability to achieve zero-voltage or zero-current switching, promised reduced switching losses and improved efficiency, thus aligning well with the goals of energy-efficient LED lighting systems.

Against this backdrop, this thesis focuses on the design, simulation, and analysis of a High-Performance Parallel Resonant Converter (HPPRC) tailored for LED driver applications. The objective is to address the limitations of existing LED driver circuits by harnessing the advantages of parallel resonant conversion. The HPPRC's ability to achieve efficient power transfer while maintaining favorable transient responses and robust control characteristics presents a compelling avenue for enhancing the performance of LED lighting systems.

By investigating the history of LED lighting technology, the evolution of LED driver circuitry, and the emergence of resonant power conversion, this research is positioned to contribute to the ongoing efforts aimed at optimizing energy consumption, enhancing lighting quality, and advancing the capabilities of LED-based illumination systems.

1.2 Problem Statement

The rapid proliferation of Light Emitting Diode (LED) technology and its integration into diverse lighting applications has underscored the importance of efficient and reliable LED driver circuits. While LED technology offers remarkable advantages in terms of energy efficiency, lifespan, and design flexibility, the realization of these benefits hinges upon the effectiveness of the associated driver circuitry.

Existing LED driver solutions, although capable of providing adequate power conversion, often grapple with inherent challenges that impede optimal performance. Traditional driver topologies, including buck and boost converters, exhibit limitations such as increased switching losses, thermal stress, and suboptimal efficiency. These shortcomings become particularly pronounced as LED applications scale up to higher power levels and demand for more stringent performance criteria.

Furthermore, the transition towards energy-efficient lighting solutions has prompted the exploration of resonant power conversion as a means to mitigate the drawbacks of conventional switching converters. Resonant converters, through their zero-voltage or zero-current switching mechanisms, promise reduced switching losses and improved efficiency. However, their successful integration into LED driver circuits necessitates careful design, control, and analysis to harness their full potential.

Therefore, the primary problem addressed by this research is the design, simulation, and analysis of a High-Performance Parallel Resonant Converter (HPPRC) specifically tailored for LED driver applications. This problem encapsulates the need to enhance the efficiency, reliability, and overall performance of LED driver circuits, particularly in the context of higher power LED lighting systems. By identifying and resolving the challenges inherent in existing solutions and capitalizing on the benefits of resonant power conversion, this research seeks to

contribute a novel driver circuitry solution that can empower the widespread adoption of energy-efficient LED lighting technologies.

1.3 Objectives

The main objectives of this thesis are as follows:

1. **Design of High-Performance Parallel Resonant Converter (HPPRC):** The primary objective is to conceive a novel HPPRC topology optimized for LED driver applications. This involves formulating a comprehensive design methodology that integrates the principles of resonant power conversion with the specific requirements of LED lighting systems, focusing on efficiency, reliability, and power quality.
2. **Simulation and Performance Analysis:** The research aims to simulate the designed HPPRC under various operational scenarios and loading conditions. This includes analyzing transient responses, steady-state behaviors, and energy transfer dynamics to quantify the converter's performance metrics, such as efficiency, power factor, and harmonic distortion.
3. **Sensitivity Analysis and Robustness Assessment:** An essential objective is to conduct sensitivity analyses to evaluate the HPPRC's tolerance to component variations and external disturbances. By quantifying the impact of manufacturing tolerances and parameter uncertainties, the research aims to ascertain the converter's robustness in real-world applications.
4. **Control Strategy Exploration:** This research seeks to explore and evaluate different control strategies for regulating the HPPRC's key parameters, such as output voltage and current. Both traditional control techniques, such as Proportional-Integral (PI) control and frequency modulation, and modern control algorithms like Model Predictive Control (MPC) and Sliding Mode Control will be investigated for their effectiveness and suitability.
5. **Comparative Performance Analysis:** The thesis intends to perform a comprehensive comparative analysis of the various control strategies employed. By assessing their performance in terms of transient response, stability, and adaptability to load variations, the research aims to identify the most suitable control approach for optimizing the HPPRC's performance in LED driver applications.
6. **Experimental Validation:** An important objective is to experimentally validate the proposed HPPRC's performance through hardware implementation. This involves developing a practical test setup, implementing the selected control strategy, and analyzing the real-world performance of the designed converter under varying conditions.

7. **Contribution to Energy-Efficient LED Lighting:** Ultimately, the research strives to contribute a validated and optimized HPPRC solution to the domain of energy-efficient LED lighting systems. By addressing the limitations of conventional LED driver circuits and harnessing the benefits of resonant power conversion, the research aims to facilitate the advancement of sustainable and high-performance LED lighting technologies.

The achievement of these objectives will collectively contribute to the development of a robust and efficient driver circuit solution for LED lighting applications, aligning with contemporary energy conservation goals and technological advancements.

1.4 Scope and Limitations

1.4.1 Scope

This thesis is focused on the design, simulation, and analysis of a High-Performance Parallel Resonant Converter (HPPRC) specifically tailored for LED driver applications. The scope of this research encompasses several key aspects:

1. **Converter Design:** The research delves into the design of the HPPRC, including the selection of component values, resonant tank sizing, and control circuitry integration. The design process accounts for LED driver requirements such as voltage and current regulation, efficiency enhancement, and power quality.
2. **Simulation and Analysis:** Simulation tools are employed to comprehensively analyze the HPPRC's behavior under varying operational conditions. This includes transient analysis to assess dynamic response, steady-state analysis for efficiency evaluation, and harmonic analysis to ensure compliance with power quality standards.
3. **Sensitivity Analysis:** The research involves evaluating the HPPRC's robustness by conducting sensitivity analyses. These analyses assess the impact of component variations, manufacturing tolerances, and external disturbances on the converter's performance, aiming to quantify its tolerance to real-world variations.
4. **Control Strategies:** Different control strategies, encompassing both traditional techniques and modern algorithms, are explored and compared in terms of their effectiveness in regulating the HPPRC's parameters. The scope extends to implementing the selected control strategy in hardware for experimental validation.
5. **Experimental Validation:** A practical experimental setup is developed to validate the performance of the designed HPPRC. The experimental validation phase involves implementing the chosen control strategy and assessing the converter's behavior under dynamic load conditions.

1.4.2 Limitations

Despite the comprehensive scope outlined above, there are certain limitations to be acknowledged:

1. **Component Variability:** While sensitivity analysis accounts for component variations, it may not encompass all real-world manufacturing variations. Limitations in the precision of components or unforeseen variations in manufacturing processes could influence the actual performance.
2. **Control System Complexity:** The research explores a range of control strategies, but the in-depth exploration of every possible control technique is beyond the scope. The effectiveness of control strategies might be influenced by practical implementation challenges not covered in this research.
3. **Practical Implementation Challenges:** The experimental validation phase might encounter challenges related to hardware constraints, transient responses, and noise that could affect the converter's performance in ways not entirely accounted for in the simulations.
4. **Application-Specific Considerations:** While the research is geared towards LED driver applications, variations in LED types, driver requirements, and lighting system configurations might necessitate additional considerations that fall outside the scope of this study.
5. **Commercialization Considerations:** The transition from a research prototype to a commercially viable product involves factors like cost-effectiveness, manufacturability, and compliance with industry standards. These aspects are beyond the scope of this research.

By acknowledging these scope and limitations, this research aims to provide valuable insights into the design, simulation, and analysis of an HPPRC for LED driver applications while recognizing the broader context in which such systems operate.

1.5 Thesis Organization

This thesis is structured to provide a systematic exploration of the design, simulation, and analysis of a High-Performance Parallel Resonant Converter (HPPRC) for LED driver applications. The organization of the thesis is as follows:

Chapter 2: Literature Review This chapter presents a comprehensive review of relevant literature in the fields of LED lighting technology, power conversion for LED drivers, and resonant power converters. It examines the evolution of LED technology, outlines the challenges of conventional LED driver circuits, and explores the theoretical foundations of

parallel resonant converters. The chapter also reviews previous research efforts and identifies gaps that this thesis aims to address.

Chapter 3: Theoretical Framework Chapter 3 lays the theoretical groundwork for the research. It introduces the basics of resonant power conversion, explains the principles of parallel resonant circuits, and discusses the design considerations specific to LED driver circuits. The proposed High-Performance Parallel Resonant Converter is introduced, detailing its topology, operation, and design methodology. The chapter also covers power flow analysis, emphasizing the integration of resonant conversion with LED driver requirements.

Chapter 4: Simulation and Modeling This chapter focuses on the simulation methodologies employed to model the HPPRC. It outlines the simulation tools used, details the modeling of the HPPRC components, and explains the transient and steady-state analysis techniques used to assess the converter's performance. Sensitivity analysis methods are elaborated upon, providing insights into the converter's robustness against parameter variations and external disturbances.

Chapter 5: Control Strategies Chapter 5 explores various control strategies tailored for the HPPRC. It covers both traditional control techniques and modern algorithms, highlighting their applicability to parameter regulation and system stability. The chapter details the implementation of control strategies, presents control algorithm pseudocode, and discusses the comparative evaluation metrics used to assess their effectiveness.

Chapter 6: Experimental Validation This chapter shifts from simulation to practical implementation. It describes the experimental setup used to validate the HPPRC's performance in a real-world scenario. The hardware implementation of the chosen control strategy is discussed, and the results obtained from experimental validation are presented and analyzed.

Chapter 7: Discussion Chapter 7 interprets the results obtained from both simulations and experimental validation. It provides an in-depth discussion of the findings, comparing the performance of the HPPRC with existing solutions. The implications of the research on LED driver applications are examined, and potential benefits, limitations, and areas for further investigation are outlined.

Chapter 8: Conclusion The final chapter summarizes the research journey and its contributions. It restates the objectives achieved, discusses the practical relevance of the findings, and emphasizes the significance of the proposed HPPRC for energy-efficient LED lighting systems. The chapter concludes with reflections on the research's broader impact and suggestions for future research directions.

Chapter 9: References This chapter lists all the references cited throughout the thesis, providing readers with a comprehensive bibliography of the sources consulted during the research.

Chapter 10: Appendices The appendices contain supplementary information, such as component datasheets, simulation parameters, and additional details that enhance the understanding of the research process.

The thesis organization outlined above ensures a coherent and structured presentation of the research, guiding the reader through the development, analysis, and validation of the High-Performance Parallel Resonant Converter for LED driver applications.

Chapter 2

Literature Survey

Resonant converters are playing a major role in different application like telecommunication and consumer electronics due to their attractive characters like high efficiency, switching capability as well as high operating frequency. Three major topologies of RC circuits are series, parallel and series-parallel combination also referred to the LLC RC. In SRC, the resonant capacitor and resonant inductor are in series. It works under ZVS condition as the operating region of the SRC is located in resonant frequency's right side. The major drawbacks of this resonant converter are high circulating energy, input voltage condition, and turn off current at the higher input voltage condition, light load regulation. In the PRC, the resonant tank is located as the series and load are located as parallel. The ZVS is achieved here by making the resonant converter to operate on the right part of the resonance frequency. The operating region of the PRC is much lower than SRC and the light load regulation issues can be rectified in PRC by keeping the output voltage regulated without changing the frequency value very often. PRC, but also suffers from the major problems like high circulating energy as well as at maximum input voltage condition; the turn off current is high. Generally, the LLC RC is the combination of PRC and SRC. The resonant tank is built with three resonant components like a resonant capacitor, resonant inductor, and parallel capacitor. The impedance matching is achieved in the LLC RC by adding an inductor filter at the output of the converter's auxiliary port. The circulating energy is lower in LLC since the load can be interlinked in series with a resonant capacitor as well as the resonant inductor. Zero Voltage Switching is achieved in the LLC resonant converter by operating it on the resonant frequency's right side. In contrast to PRC and SRC, the LLC works at higher level of frequency. The major advantages of the LLC RC are low frequency variation and lower circulating current ZVS over operating range. FHA is used for representing LLC resonant converters. Each and every rapid progress in this field cause huge issues and limitations in power conversion system that necessities the converter for accomplishing maximum power efficacy with respect to maximize the battery duration in portable products and greater power density for producing comfortable small profile as well as weightless devices. Thence, the resonant converter is considered as a significant solution for the limitations and challenges to be accomplished in order to attain efficient system. Particularly, the LLC RC is generally utilized for its applicability and efficiency. Even though LLC converter possesses several operation modes, few of them are applicable and some exposes infeasibility in real-time systems due to its huge complexity in clearing the several resonant phases as well as extorting specific DC properties. Thus, the research communities have a wide opportunity for the development of an advanced model for the enhancement of

LLC resonant converters. Generally, resonant DC/DC converter is a group of converters with LC resonant tank working as the main role in power conversion technology. Moreover, the basic ideas behind the construction of resonant converters are the circulating current available in the LC resonant circuit is controllable through modifying the frequency of operation. The main applications of the resonant converter are their capabilities to accomplish ZVS or ZCS that specifies the voltage/current to converter switches beyond zero correspondingly at the time of switching transitions.

2.1 LED Lighting Technology Overview

The advent of Light Emitting Diode (LED) technology has revolutionized the lighting industry, offering numerous advantages over traditional incandescent and fluorescent lighting sources. LEDs are solid-state devices that emit light when an electric current passes through a semiconductor material. This technology has rapidly evolved, transforming LEDs from indicator lights to highly efficient and versatile sources of illumination.

2.1.1 Key Advantages of LED Lighting

LED lighting presents several key advantages that have driven its widespread adoption:

1. **Energy Efficiency:** LEDs are exceptionally energy-efficient, converting a higher percentage of electrical energy into visible light compared to traditional lighting technologies. This efficiency translates to reduced energy consumption and lower utility bills.
2. **Long Lifespan:** LEDs have an extended operational lifespan, often lasting tens of thousands of hours. This longevity reduces maintenance and replacement costs, particularly in applications with challenging accessibility.
3. **Instantaneous On/Off:** LEDs illuminate instantaneously without warm-up times, making them suitable for applications requiring rapid switching or motion detection, such as in automotive lighting.
4. **Durability:** LEDs are solid-state devices, making them more robust and resistant to shock, vibration, and environmental factors compared to fragile incandescent or fluorescent bulbs.
5. **Color Control:** LEDs offer precise control over color temperature and intensity, enabling dynamic lighting scenarios for different applications, from warm ambient lighting to vibrant displays.
6. **Directional Light:** LEDs emit light in a specific direction, reducing the need for external reflectors or diffusers. This directional characteristic contributes to increased efficiency and reduced light pollution.

2.1.2 LED Lighting Applications

The versatility of LED technology has led to its application across various domains:

1. **General Illumination:** LEDs are extensively used for general lighting in residential, commercial, and industrial spaces. They offer the flexibility to create different lighting environments, contributing to aesthetics and energy savings.
2. **Automotive Lighting:** LEDs have become a standard choice for automotive lighting, including headlights, taillights, turn signals, and interior lighting. Their efficiency and design flexibility enhance safety and aesthetics.
3. **Display and Signage:** LEDs power digital displays, signage, and screens in applications ranging from billboards and traffic signs to television screens and mobile devices. Their brightness and color control enable vibrant visuals.
4. **Street Lighting:** LED street lighting solutions provide improved visibility, reduced light pollution, and lower energy consumption compared to traditional sodium-vapor lamps.
5. **Backlighting:** LEDs are used in backlighting applications for LCD displays, laptops, televisions, and monitors, offering energy-efficient and uniform illumination.
6. **Horticultural Lighting:** In agriculture, LEDs are employed to provide tailored light spectra for optimized plant growth, enabling year-round cultivation and higher crop yields.

2.1.3 Ongoing Advancements

Continual advancements in LED technology focus on increasing efficiency, improving color quality, enhancing thermal management, and reducing costs. Research efforts also concentrate on addressing challenges such as color consistency, flickering, and compatibility with existing lighting infrastructure.

In conclusion, LED lighting technology has redefined illumination by offering energy efficiency, long lifespan, and design flexibility. Its applications span diverse sectors, influencing everything from daily lighting needs to specialized industries. The ongoing advancements in LED technology underscore its pivotal role in shaping the future of lighting systems.

2.2 Power Conversion for LED Drivers

Efficient power conversion is essential in LED driver circuits to ensure optimal operation, maintain stable illumination, and maximize the benefits of LED lighting technology. Power conversion involves transforming the incoming electrical power to meet the voltage and current requirements of LEDs. This section explores the power conversion techniques commonly employed in LED driver circuits.

2.2.1 Converter Topologies

Several power converter topologies are utilized in LED driver circuits to achieve the required voltage and current regulation:

1. **Buck Converter:** The buck converter steps down the input voltage to provide a lower output voltage. This topology is suitable for applications where the LED voltage is lower than the input voltage.
2. **Boost Converter:** The boost converter increases the input voltage to provide a higher output voltage. This topology is employed when the LED voltage exceeds the input voltage.
3. **Buck-Boost Converter:** The buck-boost converter can step up or step down the input voltage based on load requirements, making it versatile for LED driver applications with varying voltage conditions.
4. **Flyback Converter:** The flyback converter is commonly used in isolated LED driver designs, offering galvanic isolation between input and output. It is beneficial for applications requiring electrical isolation, such as in dimmable LED drivers.

2.2.2 Control Strategies

Control strategies play a crucial role in maintaining stable LED illumination and achieving desirable characteristics in LED driver circuits:

1. **Constant Current Control:** LEDs operate most efficiently when driven by a constant current. Constant current control techniques ensure that the LED current remains stable, regardless of changes in supply voltage or load.
2. **Pulse Width Modulation (PWM):** PWM control adjusts the duty cycle of the switching signal to control the average current delivered to the LEDs. This technique enables precise dimming and color mixing.
3. **Frequency Modulation (FM):** FM control adjusts the switching frequency of the converter to regulate the LED current. It is often used to maintain constant current while accommodating variations in LED voltage.

2.2.3 Efficiency Enhancement Techniques

Efficiency is a critical consideration in LED driver circuits to minimize energy losses and ensure optimal performance:

1. **Synchronous Rectification:** In synchronous rectification, a synchronous switch replaces the diode in the rectification stage of the converter, reducing switching losses and improving efficiency.

2. **Power Factor Correction (PFC):** PFC techniques improve the power factor of the LED driver, enhancing compatibility with utility grids and minimizing harmonic distortion.
3. **Zero Voltage Switching (ZVS) and Zero Current Switching (ZCS):** ZVS and ZCS techniques minimize switching losses by ensuring that switches transition during zero voltage or zero current conditions, reducing stress on components.

In conclusion, power conversion in LED driver circuits involves selecting appropriate converter topologies, implementing efficient control strategies, and employing techniques to enhance overall efficiency. The choice of topology and control strategy depends on factors such as LED voltage and current requirements, dimming capabilities, and efficiency goals. By optimizing power conversion, LED driver circuits can deliver reliable, energy-efficient, and high-quality illumination.

2.3 Parallel Resonant Converters

Parallel Resonant Converters (PRCs) are a class of power electronic converters that utilize the resonance phenomenon to achieve efficient energy conversion. In these converters, a resonant tank circuit consisting of an inductor and a capacitor is employed to facilitate zero-voltage or zero-current switching. This unique characteristic contributes to reduced switching losses, enhanced efficiency, and improved performance, making PRCs a suitable candidate for various applications, including LED driver circuits.

2.3.1 Operating Principles

The operating principle of a PRC centers around the resonant behavior of the tank circuit. When the inductor and capacitor are carefully designed, the circuit's resonance frequency matches the operating frequency of the converter. As a result, the voltage across the resonant tank becomes sinusoidal, reducing the stress on switching components.

During operation, when the voltage across the inductor reaches zero (zero-voltage switching), or the current through the capacitor becomes zero (zero-current switching), the switches can be turned on without generating significant switching losses. This unique switching mechanism results in higher efficiency and reduced electromagnetic interference (EMI) compared to non-resonant converters.

2.3.2 Advantages and Challenges

Parallel Resonant Converters offer several advantages that make them attractive for power conversion applications:

1. **Reduced Switching Losses:** The zero-voltage or zero-current switching allows the converter switches to operate under favorable conditions, minimizing switching losses and enhancing overall efficiency.

2. **Higher Efficiency:** The inherent reduction in losses leads to improved efficiency, which is crucial for energy-conscious applications like LED lighting.
3. **Improved EMI Performance:** The sinusoidal voltage and current waveforms reduce high-frequency harmonics and EMI generation, resulting in cleaner power conversion.
4. **Stable Operation:** Resonant converters tend to exhibit stable behavior, even in the presence of variations in input voltage and load conditions.

However, PRCs also pose certain challenges:

1. **Design Complexity:** Achieving proper resonance and maintaining stability require precise design of the resonant tank circuit and control strategy.
2. **Limited Load Range:** The resonance frequency restricts the converter's operating frequency range, which can limit its load range and responsiveness to load changes.
3. **Voltage Stress:** The voltage stress across components can be higher compared to non-resonant converters, necessitating careful selection of components.

2.3.3 Applicability to LED Drivers

Parallel Resonant Converters have gained attention for LED driver applications due to their potential to address the limitations of traditional switching converters. The efficient zero-voltage or zero-current switching aligns well with the requirements for high-efficiency LED lighting systems. By carefully designing the resonant tank and control strategy, PRCs can offer improved efficiency, reduced EMI, and enhanced overall performance in LED driver circuits.

In the context of LED drivers, the resonant frequency can be adjusted to match the LED load characteristics, enabling efficient power conversion across a wide range of operating conditions. While the design and implementation of PRCs for LED drivers entail specific challenges, their potential benefits make them a promising avenue for advancing energy-efficient lighting solutions.

2.4 Previous Research and State-of-the-Art

A review of previous research and the current state-of-the-art in LED driver technologies and power conversion reveals the evolution and advancements that have shaped the landscape of energy-efficient lighting systems.

2.4.1 LED Driver Technologies

Previous research efforts have focused on enhancing LED driver technologies to improve efficiency, reliability, and overall performance. Conventional driver topologies, such as buck, boost, and buck-boost converters, have been extensively studied and optimized for LED

applications. These topologies offer reasonable power conversion efficiency and have been integrated with control strategies like PWM and current regulation for stable LED operation.

2.4.2 Resonant Power Conversion for LED Drivers

In recent years, there has been growing interest in leveraging resonant power conversion for LED driver circuits. Research in this domain has explored the application of resonant converters, including both series and parallel resonant topologies. The resonant behavior of these converters has been harnessed to achieve zero-voltage or zero-current switching, leading to improved efficiency and reduced switching losses.

State-of-the-art research has investigated the suitability of resonant converters for LED driver applications. Parallel Resonant Converters (PRCs) have emerged as a promising solution due to their ability to combine the advantages of resonant switching with the demands of LED illumination. These studies have highlighted the potential of PRCs to enhance power conversion efficiency, reduce EMI emissions, and provide stable operation in LED driver circuits.

2.4.3 Control Strategies and Digital Solutions

Advancements in control strategies have played a pivotal role in shaping LED driver technologies. Traditional control techniques, such as PWM and constant current regulation, have evolved to meet the demands of modern LED lighting systems. Moreover, the integration of digital control solutions has enabled enhanced flexibility, adaptability, and ease of implementation in LED driver circuits.

Current research explores advanced control algorithms, including Model Predictive Control (MPC) and Sliding Mode Control, to optimize the performance of resonant converters. These algorithms offer improved transient response, stability, and dynamic regulation, which are crucial for maintaining LED illumination quality.

2.4.4 Integration of Smart and IoT Capabilities

Recent trends in LED driver research include the integration of smart and Internet of Things (IoT) capabilities. LED driver systems are being designed to accommodate intelligent dimming, color tuning, and connectivity features. This integration allows for adaptive lighting schemes, energy management, and remote monitoring, contributing to the broader goal of energy-efficient and user-centric lighting systems.

In conclusion, the synthesis of previous research and the current state-of-the-art underscores the ongoing efforts to enhance LED driver technologies through resonant power conversion, advanced control strategies, and the integration of smart capabilities. The exploration of Parallel Resonant Converters for LED drivers represents a promising avenue to achieve the efficiency and performance levels required by modern energy-efficient lighting applications.

Chapter 3

Theoretical Framework

3.1 Introduction to resonant converter

Typically, a converter with an inductor capacitor resonant tank is referred to as a resonant converter. The main idea underlying the design of resonant converters is that the amount of energy present in the resonant circuit may be changed by altering the frequency at which it operates. As a result, the system is able to adjust the input such that the output voltage is what is needed. In actuality, the resonant converters are made up of three fundamental components. For an inverter, the resonant tank serves as a frequency selector. The many functionality of RCs are determined by the L-C tank's distinct resonant characteristics.

The switching network in a resonant converter is configured to contain full or half bridge structure and it is utilized for producing the square wave excitation voltage for the subsequent resonant circuit. The use of the RC tank, which exhibits sinusoidal voltage and current waveform at a few sub-intervals in the switching cycle, allows for the distribution and supply of energy. The switching frequency of PWM converters is typically equal to the L-C network resonant frequency. As a result, even at low frequency ripples, the PWM converter's single cycle voltage or current swings are still substantial. Additionally, the RC tanks play a significant role in the DC to AC inverter's ability to filter out undesirable higher order harmonics from the input square wave and generate a refined sinusoidal output. A resonant converter without a rectifier phase is suggested by AC output.

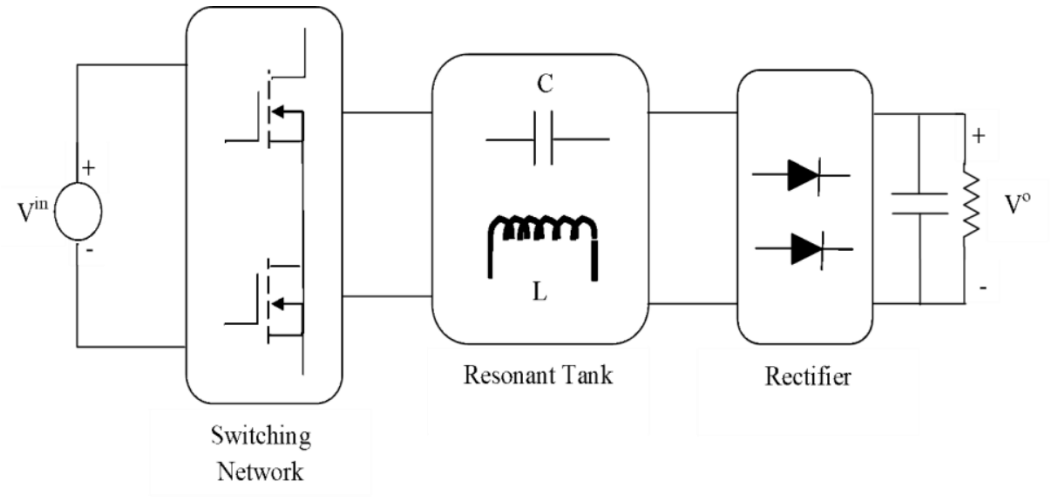

Fig.1.1 Typical model of DC-to-DC resonant converter

In terms of power efficiency and power density, the resonant converter outperforms the PWM converter. However, because the switching frequency and the resonant frequency are similar, it results in significant ripples during a switching cycle of the current waveform. In comparison, the PWM converter's waves are barely audible. As a result, the converter's components must be chosen based on the peak waves in voltage or current. Due to the tank circuit's high resonance, the current circulation inside the tank is increased, leading to additional conduction losses. As a result, the resonant converter's ability to reduce switching losses does not come at the expense of increased conduction losses. This is a significant disadvantage of the resonant converter since it makes it impossible to optimize the converter at higher loads because high efficiency cannot be achieved at lesser loads. SRC and PRC, two-component resonant converters. And the three resonant converter components, known as the SPRC, LLC, and LCC, are detailed below.

3.1.1 Series Resonant Converter

The resonant capacitor (C) and resonant inductor (L) are the two primary parts of the full-bridge SRC construction (Figure 1.2). The L and C are often connected in sequence. Additionally, the output load resistance and resonant circuit impedance (Z) are serially coupled with the resonant tank to display the function of switching frequency. As a result, a change in switching frequency might cause a change in the voltage across the output impedance. When the resonant frequency ($F = \frac{1}{2\pi\sqrt{LC}}$) is reached, the normalized output voltage gain ($M_i = \frac{niV^0}{V^{in}}$) reaches unity with zero resonant impedance. The transformer turn ratio, or ni, is set to 1 in this instance. For all switching frequencies, the resonant impedance magnitude turns out to be substantial. Greater switching frequency causes the total impedance to change from resistive to inductive in nature. This suggests that there is a delay between the input current and the input voltage, leading to ZVS. On the other hand, ZCS is brought on by capacitive impedance at frequencies below resonance. In the end, the SRC is suitable to both big input and high load systems.

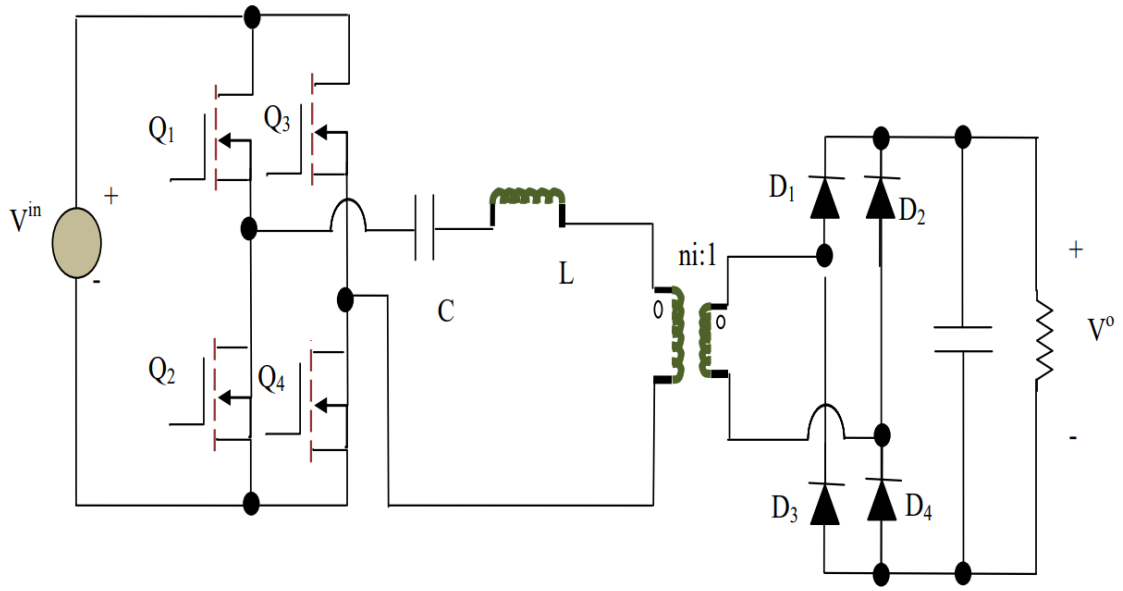

Fig. 1.2 Structure of full-bridge SRC

3.1.2 Parallel Resonant Converter

Similar to SRC, the PRC resonant tank has two resonant components: a resonant inductor and a resonant capacitor. The PRC has its capacitor parallel to the output rectifier, in contrast to the SRC, which does not. The converter resembles a current source because the L-C filter of the PRC provides an inductively coupled output. Peak gain in PRC is influenced by load resistance. The full-bridge PRC illustrates the SRC, where the resonance peak gain is typically unity and independent of load (Figure 1.3).

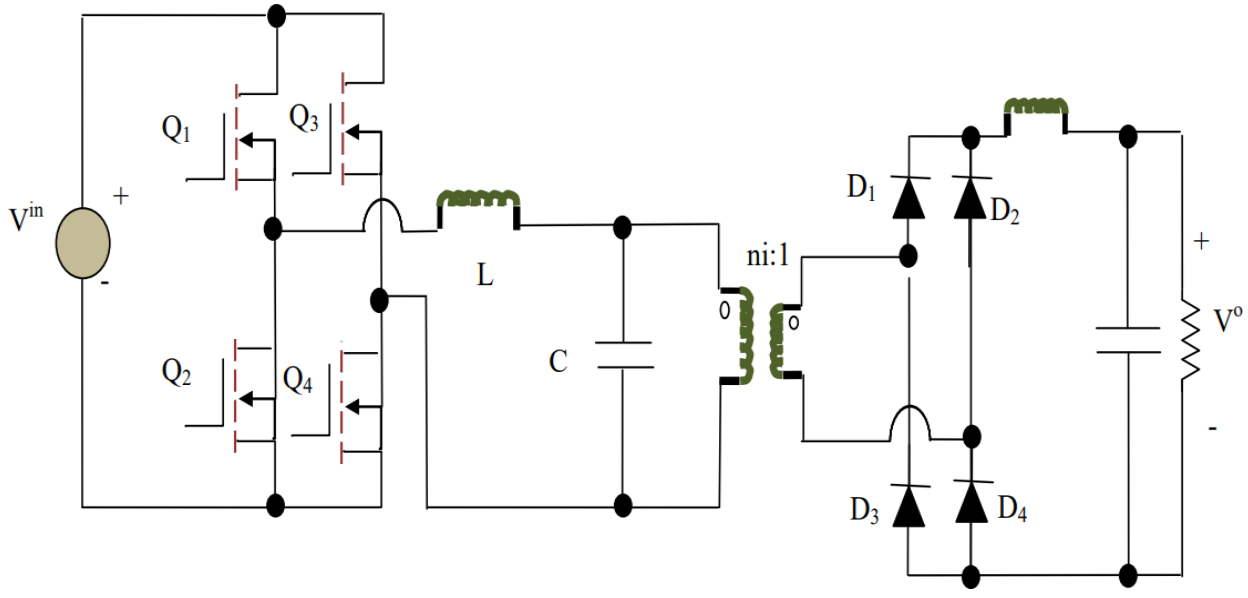

Fig. 1.3 Structure of full-bridge PRC

3.1.3 Series-Parallel Resonant Converter

SPRC is referred to as a three-component converter, which results by the integration of SRC and PRC. It is broadly categorized as LCC and LLC converters.

3.1.4 LCC Resonant Converter

Typically, there are three main resonant components in LCC, as resonant inductor L which includes Series resonant capacitor C and Parallel resonant capacitor C^p. In LCC, L and C has a series connection, and C^p is connected as parallel. Furthermore, the LCC consists of 2 resonant frequencies namely, short circuit frequency f^0 and Open circuit frequency f^∞. The frequency f^0 is determined using $f^0 = \frac{1}{2\pi\sqrt{LC}}$, and f^∞ is estimated through $\frac{1}{2\pi\sqrt{(LC \| C^p)}}$, in which $C \parallel C^p = \frac{CC^p}{C+C^p}$. Here described the full bridge LCC RC (Figure 1.4). The LCC converters can effectively handle the zero-load condition. Further, these converters impart steep slope in the gain frequency curves, under small load condition. The large resonant current that is achieved in PRC is also eliminated by this converter type.

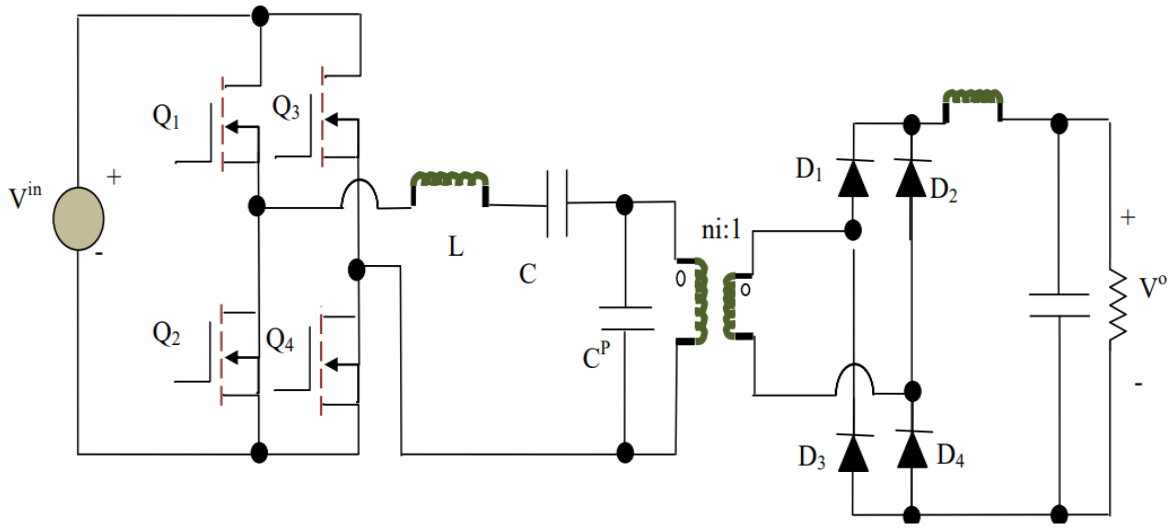

Fig. 1.4 Structure of full-bridge LCC resonant converter

3.1.5 LLC Resonant Converter

Typically, it is a 3 component Resonant Converter. In contrast to the LCC converter, the LLC contains a magnetizing inductor L^m, located in parallel to the rectifier input. The components in LLC are Series resonant inductor L, Series resonant capacitor C and Parallel/magnetizing resonant inductor L^m The only difference between the LCC and the LLC RCs' are depicted in Fig. 1.5.

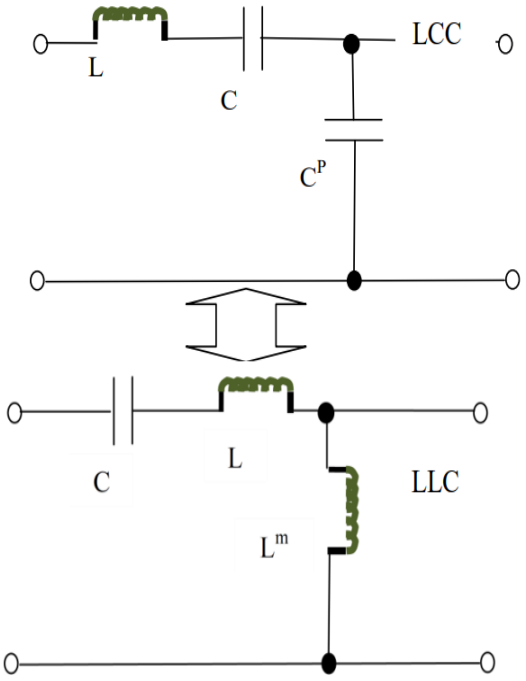

Fig.1.5 Structure of full-bridge LCC and LLC resonant DC to DC converter

The inductor L^m formed from the primary transformer side, which is implemented via the transformer magnetizing inductor. Since every transformer owns a magnetizing inductor, the LCC resembles SRC. However, L^m in SRC fails to cause resonance because it is greater than the resonant inductor (L). In contrast, in LLC, L^m has relatively comparable inductance to L. Therefore, L^m of LLC will certainly cause resonance to happen. The common components in the LLC Resonant Converter represents the structure of half-bridge LLC Resonant Converter (Figure 1.6 and Figure 1.7).

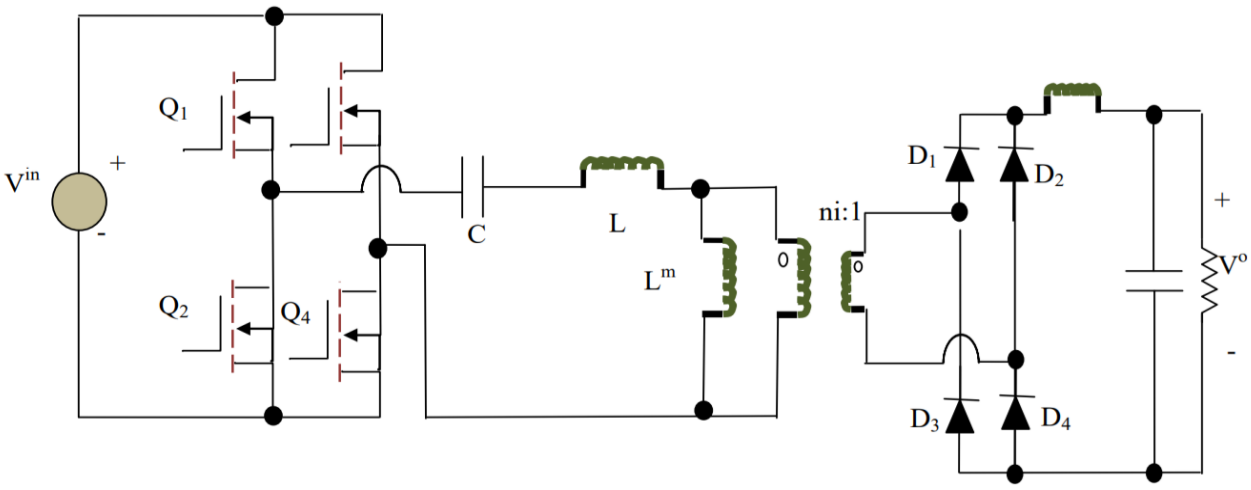

Fig.1.6 Structure of full-bridge LLC resonant DC-DC converter

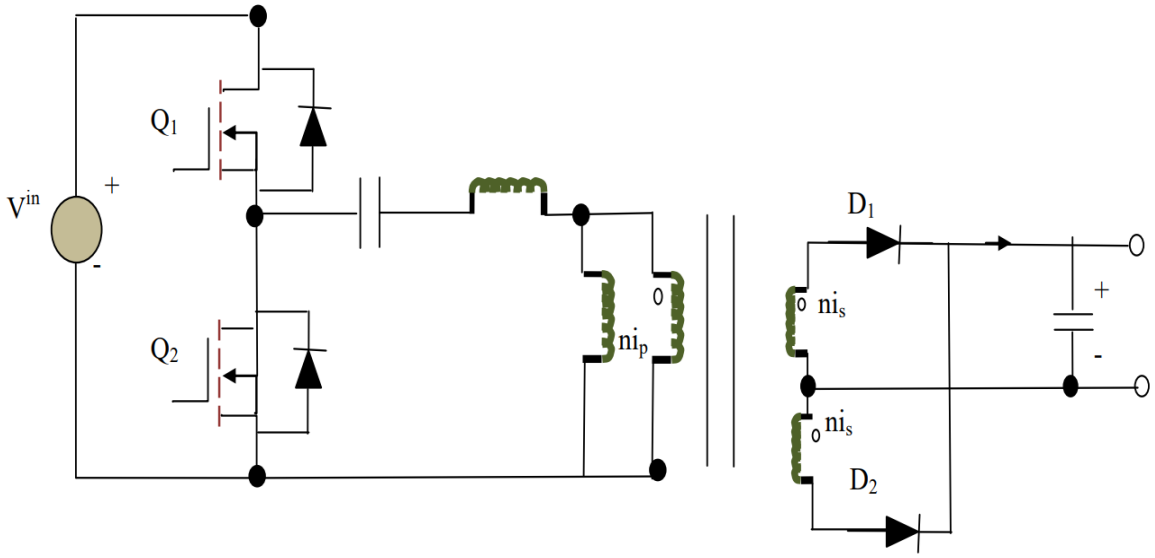

Figure 1.7: Structure of half-bridge LLC resonant converter

Similar to the LCC RC, the LLC RC has 2 resonant frequencies. i.e., open circuit (f^{∞}) and short circuit (f^{0}) The term $f^{\infty}$is estimated using $f^{\infty} = \frac{1}{2\pi\sqrt{(L+L^{m})C}}$ and f^{0} is computed through $f^{\infty} = \frac{1}{2\pi\sqrt{LC}}$. In LLC, the value of f^{0} is greater than f^{∞} , (Figure 1.6).

3.2 Operational modes of LLC resonant converter

Finding an expression that is universally correct and appropriate for all operating settings is impossible due to the constraints that emerged during the analysis of the LLC converter. As a result, in LLC, the entire operation is divided into several operating modes and each mode is individually examined. In LLC, the process is divided into numerous resonant stages for a switching cycle, with each phase's configuration being customized. To extract the precise current and voltage waveforms for each mode of operation, distinct expressions are generated separately. The base coefficients listed below are used to normalize the circuit characteristics such as power, voltage, current, and frequency in order to provide a more comprehensive evaluation, in which

$Z = \sqrt{\frac{L}{C}}$.

- Base power: $P^{base} = \frac{(niV^{0})^{2}}{Z}$
- Base voltage: $V^{base} = niV^{0}$
- Base current: $I^{base} = \frac{niV^{0}}{Z}$
- Base frequency: $f^{base} = \frac{1}{2\pi\sqrt{LC}}$

The parameters in this case that have been divided by the appropriate base coefficients are referred to as normalized parameters and are denoted by the symbol ni. The base frequency is used here instead of the resonant frequency, which denotes the frequency f^{base} at which the resonant tank produces its peak output response.

3.2.1 Resonant Phases

Typically, the LLC resonant tank has a dual resonant model. Here, the resonance is created through L and C or along with L_m. Various resonant phases are determined using the voltage condition and the switching state of the resonant converter. There are 6 possible phases in LLC. The LLC is set as 50% duty cycle and the voltage regulation is accomplished using the variable frequency control. Hence, the resonant tank waveforms are symmetrically reversed for one half of the switching cycle, as in the other half cycle. In order to make the evaluation easier, only the half switching cycle is taken into account. The resonant tank input voltage is set positive for full bridge LLC. Hence, Q_1 and Q_3 is kept switched on, while Q_2 and Q_4 is kept switched off. In contrast, for half bridge Resonant Converter, the upper switch is turned on. Based on the voltage conditions at L_m , there exist 3 resonant phases as stated below.

Cut-off phase, $V^m = niV^0$(also referred to as phase O)

Negative clamped phase, $V^m = -niV^0$(also referred to as phase N)

Positive clamped phase, $V^m = niV^0$ (also referred to as phase P)

3.3 Traditional LLC Operation Analysis

The LLC RC is highly beneficial by the applications, involving switching mode power supply to obtain high rated power density and efficacy. Yet, the LLC RCs' are difficult to be analysed. The reason is its complicated topology and the non-availability of suitable means to analyse the operation and properties of the LLC resonant elements. However, three models were introduced to generalize the topology of LLC resonant converters with unique analytical procedures, as given below

3.3.1 Frequency Domain Analytical Model

In the analysis of frequency domain, the topology is simplified by making use of sinusoidal waveform estimations, with no much consideration on accuracy. This model does not represent the differences in operational modes via solving the transfer operations.

Basically, when a resonant converter topology is considered, the voltage excitation signal of the resonant tank is the square-waves that are produced by the preceding switch network. Eliminating the higher order harmonics in the square wave aids in yielding the AC equivalent circuit, which make the analysis to be simpler. The transfer function of the RC tank and the output rectifier phase is then achievable using the frequency domain response. Additionally, the DC properties owned by the converter can also be obtained. This frequency domain approach is termed as FHA. The input voltage in V is same for the square wave voltage at the input in a full bridge switching network. In contrast, in a half bridge switch network, the input voltage becomes half in V. In order to generalize the evaluation, the full bridge configuration is analysed and the resultant is transformed to half bridge form by just replacing in V as in V 2 In addition to this, the AC circuit load resistance is required to be included. This is done by transforming it into AC impedance, at the primary side of the transformer. The LLC RC's AC equivalent circuit depicts the formation of equivalent load impedance AC R (Fig. 1.8 and 1.9).

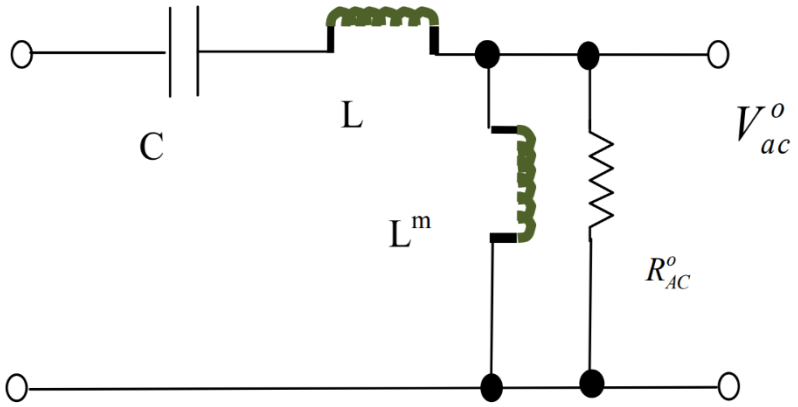

Fig. 1.8: LLC resonant converter AC equivalent circuit

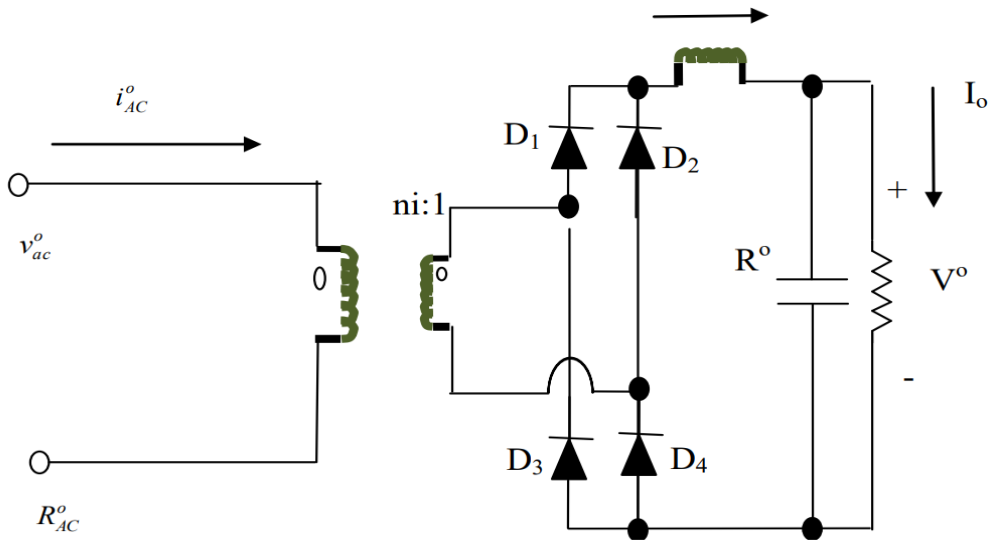

Fig. 1.9: Formation of equivalent AC load impedance R^{AC}

3.3.2 State-Plane Analytical Model

This analytical model is the one that exploits a state plane diagram to specify the link between various parameters. In order to attain steady-state performance, a closed loop trajectory is formed on the state plane. The model provides the converter gain and it is also used to analyse the various resonant topologies. This model consists of a three-dimensional space by utilizing the state parameters such as $i^r, i^m \; and \; v^m$. The resonant tank has 6 various phases and for each phase, the singular point can be obtained. The singular point acts as the middle point for the piecewise trajectory of the resonant phases. The equivalent circuit for the LLC resonant phase, called PO (Figure 1.10).

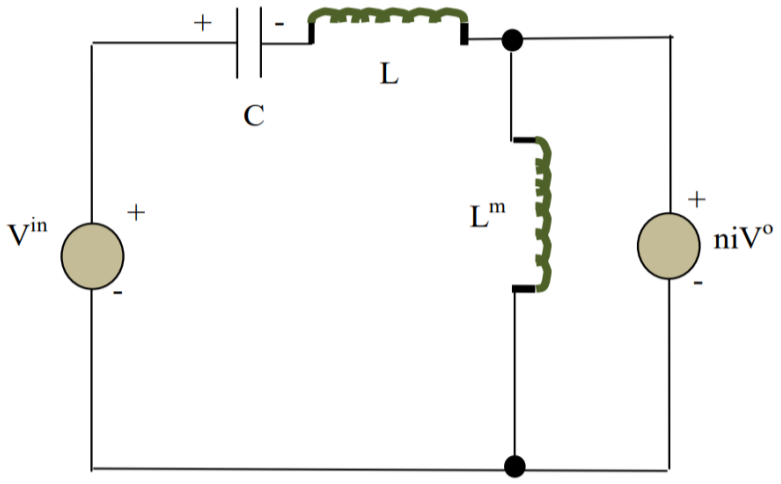

Fig. 1.10: The equivalent circuit of LLC Resonant Converter at Phase PO

3.3.3 Time-Domain Analytical Model

The time-domain analytical model concentrates on the characteristics of the resonant converter in its time-domain. It operates on the cyclic resonate current and voltage waveforms, with respect to the various resonant operational modes and resonant phases. The system gains configure the operations as buck or boost, depending on DCM/CCM and switching frequency. However, the boundaries of operation between different LLC operational modes are fuzzy that the relation between the gain of the converter and the frequency of switching per load power is unavailable.

3.4 The Design procedure of LLC

On considering the complexities caused by the operational modes and analysis models, LLC focus on the peak gain points to attain improved performance. While designing an LLC, the peak gain occupies a significant role because it specifies the ability of the converter in regulating the voltage. The smallest feasible operating frequency is the switching frequency at peak gain point. The LLC converter should operate above the peak gain frequency to remain in Zero Voltage Switching. The reason is that the peak gain serves as a boundary between ZCS and ZVS. Even though several techniques were introduced to enhance the prediction accuracy and generalize the calculations, none of the models can be recognized as effective and direct to simplify the LLC resonant converter operations. Typically, the approximation model offers peak gain, according to the switching frequency and load power values. However, it has to be suitably utilized for achieving better performance of the LLC converter.

Chapter 4

Brief Review of Resonant Converters

Resonant-converter topologies come in a wide variety, but they all function basically the same way: By using power switches, a resonant circuit receives a square pulse of voltage or current.The output is supplied by tapping off some or all of the energy that is circulating in the resonant circuit.The references cited in this subject provide more thorough explanations and debates.

The series resonant converter (SRC), seen in Fig. 2.1a, and the parallel resonant converter (PRC), depicted in Fig. 2.1b, are the two fundamental forms of resonant converters. Both of these converters control their output voltage by varying the driving voltage's frequency, which alters the resonant circuit's impedance.

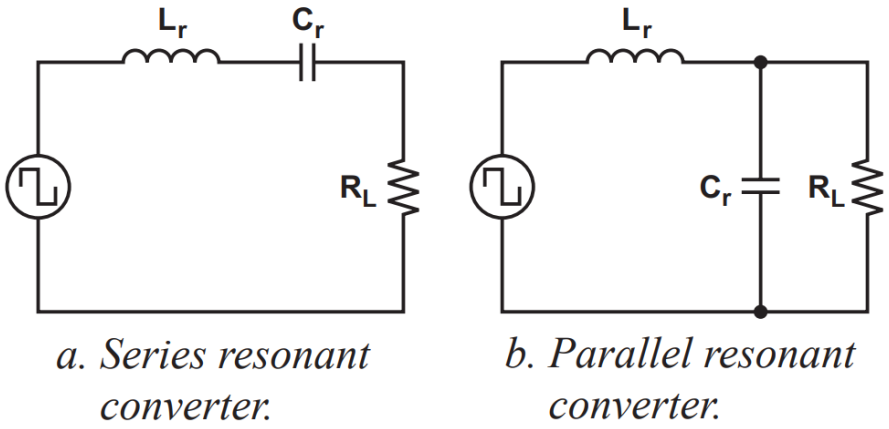

Fig. 2.1. Basic resonant-converter configurations.

The load and its impedance share the input voltage. An SRC's DC gain is never more than one since it acts as a voltage divider between the input and the load. It is challenging to regulate the output when the load is light because the load's impedance is very high relative to the resonant circuit's impedance and doing so necessitates that the frequency approach infinity as the load decreases. When there is a wide input-voltage range, substantial frequency variation is necessary to regulate the output, even at minimal loads. Due to the load's parallel connection to the resonant circuit in the PRC depicted in Fig. 1b, a significant amount of circulating current is unavoidably needed. In applications with high power density or significant load changes, this makes it challenging to utilize parallel resonant topologies.

4.1 LCC and LLC Resonant Converters

A series-parallel resonant converter (SPRC), which combines the parallel and series designs, has been proposed as a solution to these restrictions. One variation of this arrangement, as seen in Fig. 2.2a, employs an LCC layout, which is one inductor and two capacitors. Despite the fact that this combination addresses the shortcomings of a single SRC or PRC by including additional resonant frequencies, it necessitates two separate physical capacitors, each of which is enormous and costly due to the high AC currents. The SPRC may be modified to employ two inductors and one capacitor, making an LLC resonant converter (Fig. 2.2b), to provide comparable properties without altering the physical component count. One benefit of the LLC topology over the LCC topology is that the two physical inductors—the series resonant inductance, L_r, and the transformer's magnetizing inductance, L_m—can frequently be combined into a single physical component.

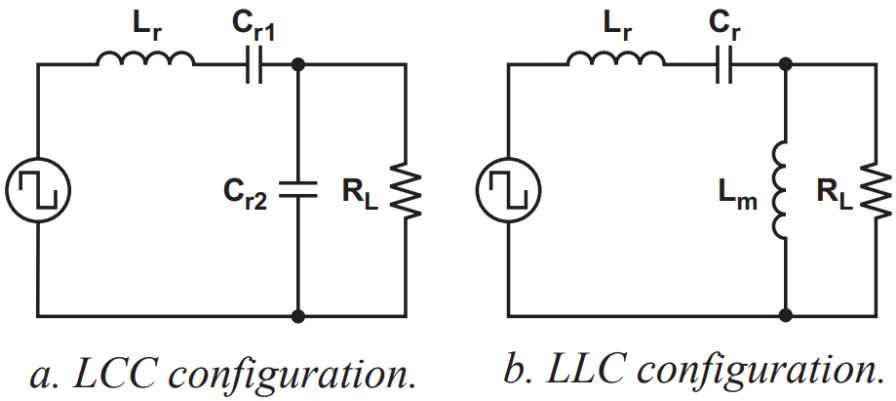

Fig. 2.2. Two types of SPRC

Compared to traditional resonant converters, the LLC resonant converter offers a number of extra advantages. For instance, it can adjust the output while retaining outstanding efficiency over extensive line and load fluctuations with a relatively modest difference in switching frequency. Additionally, across the full working range, it can perform zero voltage switching (ZVS). The method for constructing this topology will next be discussed, followed by a description of how to use the LLC resonant configuration in an isolated half-bridge topology.

4.2 LLC resonant Half-Bridge Converter

This section discusses a typical isolated LLC resonant half-bridge converter's functioning, simplified circuit modeling, and the voltage-gain function, which represents the relationship between the input and output voltages. The design process presented in this article is built on this voltage-gain function.

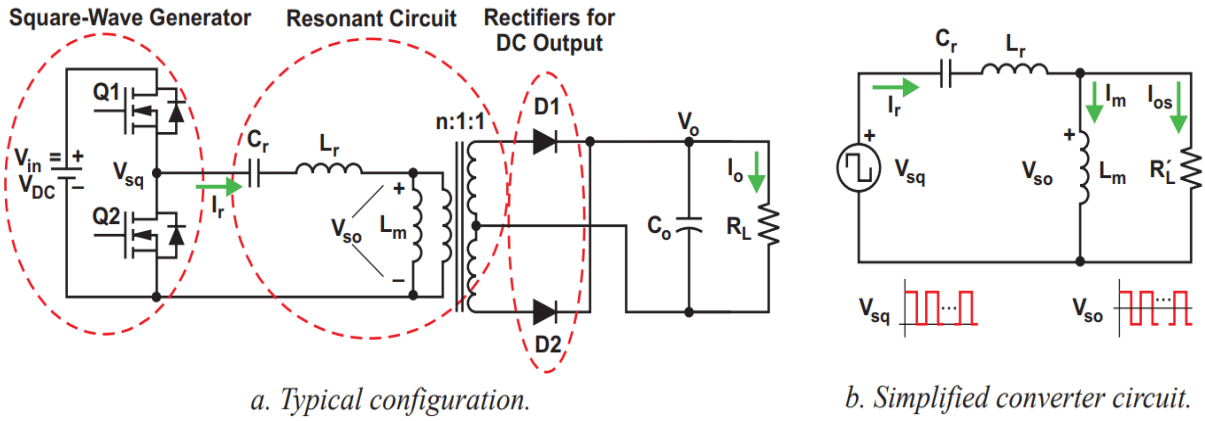

a. Typical configuration. *b. Simplified converter circuit.*

Fig. 2.3. LLC resonant half-bridge converter.

4.2.1 Configuration

A typical topology for an LLC resonant half-bridge converter is shown in Fig. 3a. This circuit and that in Fig. 2.2b are extremely similar. For ease of use, Fig. 2.2b is reproduced as Fig. 2.3b with the series elements switched around, allowing for a direct comparison with Fig. 3a. There are three primary components to the converter arrangement in Fig. 2.3a:

1. Typically, MOSFET power switches Q1 and Q2 are arranged to create a square wave generator. This generator operates switches Q1 and Q2 with alternating 50% duty cycles to generate a unipolar square-wave voltage, Vsq. In order to prevent cross conduction and give time for ZVS to be established, there has to be a little dead period between each transition.

2. The resonant capacitance makes up the resonant circuit, also known as a resonant network, C_r, and two inductances—the series resonant inductance, L_r, and the transformer's magnetizing inductance, L_m. The transformer turns ratio is n. The resonant network circulates the electric current and, as a result, the energy is circulated and delivered to the load through the transformer. The transformer's primary winding receives a bipolar square-wave voltage, V_{so}. This voltage is transferred to the secondary side, with the transformer providing both electrical isolation and the turns ratio to deliver the required voltage level to the output. In Fig. 2.3b, the load R′ L includes the load RL of Fig. 2.3a together with the losses from the transformer and output rectifiers.

3. To convert AC input to DC output and power the load RL, a full-wave rectifier made up of two diodes is used on the converter's secondary side. The output capacitor tames the voltage and current that have been rectified. A capacitive output filter and a full-wave bridge arrangement are two ways to design the rectifier network. In order to decrease conduction losses, the rectifiers can also be used in low-voltage and high-current applications. This method is known as synchronous rectification.

4.2.2. Operation

This section provides a review of LLC resonant-converter operation, starting with series resonance.

***Resonant Frequencies in an SRC*:**

Fundamentally, the resonant network of an SRC exhibits a minimal resistance to the sinusoidal current at the resonant frequency independent of the frequency of the square-wave voltage given at the input. This is also known as the resonant circuit's selective feature. Away from resonance, the circuit displays rising impedance values. The amount of current, or associated energy, that will be circulated and delivered to the load is then determined by the value of the resonant circuit's impedance at that frequency for a certain load impedance. To control how much energy is delivered to the load, the square-wave generator's frequency causes the resonant circuit's impedance to change.

An SRC has only one resonance, the series resonant frequency, denoted as –

$$f_0 = \frac{1}{2\pi\sqrt{L_r C_r}} \tag{1}$$

The circuit's frequency at peak resonance, $fc0$, is always equal to its f_0. Because of this, an SRC requires a wide frequency variation in order to accommodate input and output variations.

f_{c0}, f_0, and f_p in an LLC Circuit:

However, the LLC circuit is different. After the second inductance (L_m) is added, the LLC circuit's frequency at peak resonance (f_{c0}) becomes a function of load, moving within the range of $f_p \leq f_{c0} \leq f_0$ as the load changes. f_0 is still described by Equation (1), and the pole frequency is described by

$$f_p = \frac{1}{2\pi\sqrt{(L_r+L_m)C_r}} \tag{2}$$

At no load, $f_p = f_{c0}$. As the load increases, fc0 moves towards f0. At a load short circuit, fc0 = f0. Hence, LLC impedance adjustment follows a family of curves with $f_p \leq f_{c0} \leq f_0$, unlike that in SRC, where a single curve defines $f_{c0} = f_0$. This helps to reduce the frequency range required from an LLC resonant converter but complicates the circuit analysis. It is apparent from Fig. 2.3b that f_0 as described by Equation (1) is always true regardless of the load, but fp described by Equation (2) is true only at no load. Later it will be shown that most of the time

an LLC converter is designed to operate in the vicinity of f_0. For this reason and others yet to be explained, f0 is a critical factor for the converter's operation and design.

Operation At, Below, and Above f_0 :

The connection between the switching frequency (f_sw) and the series resonant frequency (f_0) may be used to describe how an LLC resonant converter operates. With the switching frequency at, below, or above the series resonant frequency, Fig. 2.4 shows the usual waveforms of an LLC resonant converter. In the graphs, the Q1 gate (Vg_Q1), Q2 gate (Vg_Q2), switch-node voltage (V_sq), resonant circuit current (Ir), magnetizing current (Im), and secondary-side diode current (Is) are displayed from top to bottom. It should be noted that the magnetizing current only flows on the main side, therefore its contribution to the power transmitted from the primary-side source to the secondary-side load is negligible. The primary-side current is just the sum of the secondary-side current and the magnetizing current, also referred to as the primary.

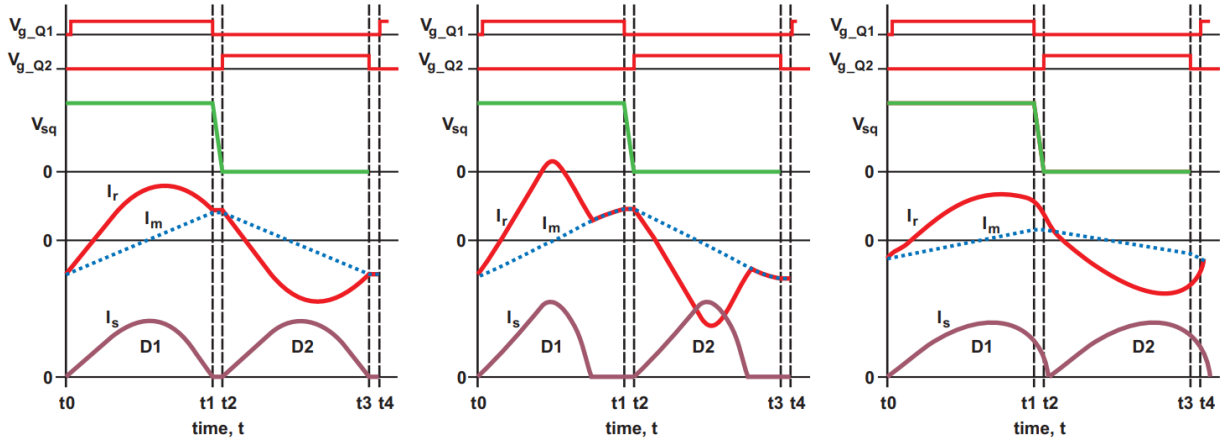

a. At f_0. *b. Below f_0.* *c. Above f_0.*

Fig. 2.4. Operation of LLC resonant converter

Operation at Resonance (Fig. 2.4a):

The series resonant frequency and the switching frequency are identical in this mode. No further power is supplied to the secondary side once switch Q1 is closed since the resonant current and the magnetizing current are equal. The circuit accomplishes primary-side ZVS and obtains a moderate commutation of the rectifier diodes on the secondary side by delaying the time at which switch Q2 switches on. We'll address the requirements for obtaining ZVS later. However, it is clear that using series resonance only results in one operational point. To account for input and output changes, the switching frequency will need to be changed away from resonance.

Operation Below Resonance (Fig. 2.4b):

Because the resonant current arrived at the magnetizing current's value before the driving pulse width finished in this case, the power transfer ceases even though the magnetizing current continues. Even yet, it is still feasible to achieve primary ZVS and secondary soft commutation

of the rectifier diodes by operating below the series resonant frequency. The secondary-side diodes must run in discontinuous current mode in order to deliver the same amount of energy to the load, which raises the amount of circulating current in the resonant circuit. This greater current causes higher conduction losses on both the primary and secondary sides. It should be kept in mind, though, that the primary ZVS risked being lost if the switching frequency dropped too low. This will lead to significant switching losses and a number of related problems. This will be clarified later...

Operation Above Resonance (Fig. 2.4c):

The primary side of the resonant circuit displays a lower circulating current in this mode. This minimizes conduction loss since the resonant circuit's current operates in the continuous-current mode, producing a lower RMS current for the same amount of load. Primary ZVS can be attained while running above the resonance frequency, despite reverse recovery losses and rough commutation of the rectifier diodes. Operation exceeding the resonance frequency may cause significant frequency increases in low-load scenarios. The explanation above has demonstrated that the converter may be created using either $f_{sw} \geq f_0$ or $f_{sw} \leq f_0$, or by varying f_{sw} on either side around f_0. Further discussion will show that the best operation exists in the vicinity of the series resonant frequency, where the benefits of the LLC converter are maximized. This will be the design goal.

4.3. Modelling an LLC Half-Bridge Converter

A voltage transfer function is necessary when designing a converter for variable energy transfer and output voltage adjustment. The mathematical link between the input and output voltages is represented by the transfer function, also known as the input-to-output voltage gain in this context. This section will outline the features of the gain and how the gain formula was created. Later, the resulting gain formula will be applied to define the LLC resonant half-bridge converter design process[28].

All variables must be described by equations guided by the LLC converter architecture depicted in Fig. 2.5a in order to create a transfer function. The transfer function is then obtained by solving these equations. State space averaging and other conventional techniques have been successful in modelling pulse-width-modulated switching converters, but when it comes to resonant converters, they have proven ineffective, leading designers to look for other strategies.

Modelling with Approximations:

As already mentioned, in close proximity to series resonance, the LLC converter was in operation. This indicates that the series resonant frequency is being reached by the primary component of circulating current in the resonant network. This gives an indication that the circulating current is pure sinusoidal current and comprises mostly of a single frequency. Even while this assumption is not entirely correct, it comes close, especially when the switching cycle of the square wave coincides with the series resonant frequency. What about the mistakes, though? In reality, more frequency components are included if the square wave deviates from the series resonance; however, it is possible to make an approximation using the square wave's

single fundamental harmonic while ignoring all higher order harmonics and putting any potential accuracy concerns on hold for the time being. This is the so-called first harmonic approximation (FHA) approach, which is now used for designing resonant converters. As long as the converter performs at or near the series resonance, this strategy yields acceptable design outcomes. Gain, also known as the input-to-output voltage-transfer function, may be developed using the FHA approach. The initial phases in this procedure are as follows:

- Represent the voltage and current of the primary-input unipolar square wave using only their primary constituents, omitting higher-order harmonics.
- Ignore the effect from the output capacitor and the transformer's secondary-side leakage inductance.
- Refer the obtained secondary-side variables to the primary side.
- Represent the referred secondary voltage, which is the bipolar square-wave voltage (Vso), and the referred secondary current with only their fundamental components, again ignoring all higher-order harmonics.

With these steps accomplished, a circuit model of the LLC resonant half-bridge converter in Fig. 5a can be obtained (Fig. 2.5b). In Fig. 2.5b, V_{ge} is the fundamental component of V_{sq}, and V_{oe} is the fundamental component of V_{so}. Thus, the nonlinear and non-sinusoidal circuit in Fig. 5a is approximately transformed into the linear circuit of Fig. 2.5b, where the AC resonant circuit is excited by an effective sinusoidal input source and drives an equivalent resistive load. In this circuit model, both input voltage V_{ge} and output voltage V_{oe} are in sinusoidal form with the same single frequency— i.e., the fundamental component of the square wave voltage (V_{sq}), generated by the switching operation of Q1 and Q2. This model is called the resonant converter's FHA circuit model. It forms the basis for the design example presented in this topic. The voltage-transfer function, or the voltage gain, is also derived from this model, and the next section will show how. Before that, however, the electrical variables and their relationships as used in Fig. 2.5b need to be obtained[28].

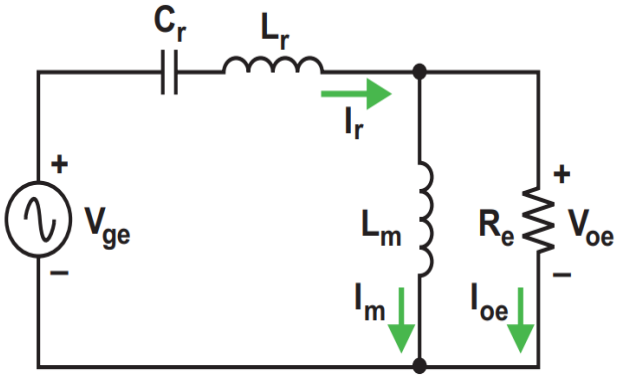

Fig. 2.5. Model of LLC resonant half-bridge converter

Relationship of Electrical Variables:

On the input side, the fundamental voltage of the square-wave voltage (V_{sq}) is,

$$V_{ge}(t) = \frac{2}{\pi} \times V_{DC} \times \sin(2\pi f_{sw} t)\,, \tag{3}$$

and its RMS value is,

$$V_{ge} = \frac{\sqrt{2}}{\pi} \times V_{DC} \tag{4}$$

RMS output current is

$$I_{oe} = \frac{2\sqrt{2}}{\pi} \times \frac{1}{n} \times I_0 \tag{5}$$

Equivalent load resistance, R_e, can be calculated a

$$R_e = \frac{V_{oe}}{I_{oe}} = \frac{8 \times n^2}{\pi^2} \times \frac{V_0}{I_0} = \frac{8 \times n^2}{\pi^2} \times R_L \tag{6}$$

Fig. 2.5, is a single-frequency, sinusoidal AC circuit, the calculations can be made in the same way as for all sinusoidal circuits.

The angular frequency is

$$\omega_{sw} = 2\pi f_{sw} \tag{7}$$

which can be simplified as

$$\omega = \omega_{sw} = 2\pi f_{sw} \tag{8}$$

The capacitive and inductive reactance of C_r, L_r, and L_m, respectively are,

$$X_{C_r} = \frac{1}{\omega C_r}, \quad X_{L_r} = \omega L_r \, , and \quad X_{L_m} = \omega L_m \tag{9}$$

The circulating current in the series resonant circuit is

$$I_r = \sqrt{{I_m}^2 + {I_{oe}}^2} \tag{10}$$

With the relationships of the electrical variables established, the next step is to develop the voltage gain function.

4.4. Voltage-Gain Function

Naturally, the relationship between the input voltage and output voltage can be described by their ratio or gain:

$$V_{g\_DC} = \frac{n \times V_0}{V_{in}/2} = \frac{n \times V_0}{V_{DC}/2} \tag{11}$$

As described earlier, the DC input voltage and output voltage are converted into switching mode, and then Equation (11) can be approximated as the ratio of the bipolar square-wave voltage (V_{sq}) to the unipolar square-wave voltage (V_{so}):

$$V_{g\_DC} \approx V_{g\_sw} \approx \frac{V_{so}}{V_{sq}} \tag{12}$$

The AC voltage ratio, V_{g_AC}, can be approximated by using the fundamental components, V_{ge} and V_{oe}, to respectively replace V_{sq} and V_{so} in Equation (12):

$$V_{g\_DC} = \frac{n \times V_0}{V_{in}/2} \approx V_{g\_sw} = \frac{V_{so}}{V_{sq}} \approx V_{g\_AC} = \frac{V_{oe}}{V_{ge}} \tag{13}$$

To simplify notation, Mg will be used here in place of M_{g_AC}. From Fig. 2.5b, the relationship between V_{oe} and V_{ge} can be expressed with the electrical parameters L_r , L_m , L_m , and R_e. Then the input-to-output voltage-gain or voltage-transfer function becomes

$$M_g = \frac{V_{oe}}{V_{ge}} = \left| \frac{jX_{L_m} || R_e}{(jX_{L_m} || R_e) + j(X_{L_r} - X_{C_r})} \right|$$

$$= \left| \frac{(jwL_m) || R_e}{(jwL_m) || R_e + jwL_r + \frac{1}{jwC_r}} \right| \tag{14}$$

Where $j = \sqrt{-1}$.

Accepting the approximation as accurate allows Equation (15) to be written:

$$V_0 = M_g \times \frac{1}{n} \times \frac{V_{in}}{2} \tag{15}$$

In other words, output voltage can be determined after M_g, n, and V_{in} are known.

Normalized Format of Voltage-Gain Function:

The normalized frequency is,

$$F_n = \frac{F_{sw}}{f_0} \tag{16}$$

Further, to combine two inductances into one, an inductance ratio can be defined as

$$L_n = \frac{L_m}{L_r} \tag{17}$$

The quality factor of the series resonant circuit is defined as

$$Q_e = \frac{\sqrt{L_r / C_r}}{R_e} \tag{18}$$

Notice that F_n, L_n, and Q_e are no-unit variables. With the help of these definitions, the voltage-gain function can then be normalized and expressed as

$$M_g = \left| \frac{L_n \times f_n^2}{[(L_n + 1) \times f_n^2 - 1] + j[(f_n^2 - 1) \times f_n \times Q_e \times L_n]} \right| \tag{19}$$

The relationship between input and output voltages can also be obtained from Equation (19):

$$V_0 = M_g \times \frac{1}{n} \times \frac{V_{in}}{2} = M_g(f_n, L_n, Q_e) \times \frac{1}{n} \times \frac{V_{DC}}{2} \tag{20}$$

where $V_{in} = V_{DC}$.

Chapter 5

Proposed Methodology

5.1 Introduction

Arc welding, battery chargers, high-voltage power supply, light-emitting diode (LED) drivers, and laser diode drivers are a few of the uses for CONSTANT current (CC) resonant converters. Conventional resonant LLC converters can accomplish CC functioning by employing a series current regulator or a tight voltage feedback and pulse frequency modulation (PFM) control [9], [10], or [11]. A converter's efficiency has a narrow operating range, even though the switching frequency's range of variation is large. Furthermore, it is impossible to optimize the size of the passive components. Reconfigurable topologies are being researched in order to reduce the switching frequency range of the LLC converter [12], [13], and [14]. Auxiliary switches in these topologies allow the input voltage amplitude of the resonant network to be switched between various levels in accordance with the necessary conversion ratio. The operating switching frequency range is lowered as a result. The primary limitations, however, are the need of many semiconductor devices and the abrupt switching action of the auxiliary switches. If LLC resonant networks are constructed around the parallel resonant frequency, they can have an inherent CC functioning with a restricted range of switching frequency fluctuation. Additional components are needed to provide the soft switching function since the zero-voltage switching (ZVS) turn-ON condition of the primary switches is no longer present [6]. The switching frequency range can be narrowed or constant frequency operation can be attained by combining buck, boost, and buck-boost topologies with a resonant network [15], [16], [17].

To achieve constant frequency operation for LED driver applications, coupled buck-LLC architecture is examined in [15]. During converter operation, hard switching is employed, and the output current is managed by the duty cycle of a buck front-end stage. [16] combines a boost converter with a twin LLC-based resonant converter for uses in automotive LED driver

technology. The boost converter is used as the front-end stage to deliver a high number of series LEDs, producing a step-up conversion ratio. Despite the use of two distinct transformers, PFM is still used to control the output current. [17] combines a fixed frequency series resonant converter with a buck-boost converter. By switching the inverter-side switches between full-bridge and half-bridge topologies, three distinct voltage gain levels may be produced in this architecture. Although this design uses ZVS, the cascaded structure lowers efficiency.

The intrinsic CC characteristic may be present at the resonance frequency in some resonant structures, such as LCL, LCC, and their derivatives, which are sometimes referred to as immittance networks. These topologies are ideal for applications using LED drivers [18], [19], [20], [21], [22], and [23]. [18] provides a multistring LCL with duty cycle control to enable fixed frequency operation. The right resonant element design can lower the circulating current. However, due to the employed duty cycle control's limitations, it cannot adjust to significant changes in the input voltage and load circumstances. [19] presents a single-stage LED driver with a half bridge CLCL converter. In a bridgeless power factor correction (PFC) stage, it uses two boost converters. Compared to an LLC converter, the switching frequency variation is less. Although total efficiency is reduced by the cascaded architecture, the CLCL resonant network's intrinsic CC property is not utilized.

Additionally, the architecture as it is currently created cannot be used for applications that need a wide variety of input and output voltages. In the LCL-based resonant LED drivers shown in [20] and [21], the output current is adjusted by adjusting the phase-shift between the gate signals of the inverter and rectifier switches. At the resonance frequency, these gadgets' function. However, when the converter operates across a wide input and output range, the phase-shift value affects the switch's ZVS range and imposes extra circulation loss.

A two-stage LED driver using a frontend buck-boost and an LCL resonant converter is provided in [22]. While the inverter switches of the resonant converter work at the resonant frequency to obtain the CC property, the output current is managed using buck-boost switches. Although this architecture can accommodate several outputs, the cascaded structure causes the component count to be high and the converter efficiency to be low.

A nonisolated resonant converter for use with LED driver applications is shown in this article. The proposed resonant network is an extension of the conventional LCL tank in which a small resonant capacitor is employed in place of the essential dc blocking capacitor to provide a new degree of freedom for better optimizing the soft switching range and the inverter switches rms current. At the rectifier step, a single auxiliary switch is placed to keep the operating frequency stable and regulate the output current using pulse width modulation (PWM). The suggested converter gains from an innate CC property that uncouples the output current from the load circumstances.

The auxiliary switch can also provide PWM dimming and open-load prevention. The recommended LED driver benefits from both the ZVS turn-on and ZVS turn-off functionality of the switches over a wide range of input and output voltages. In Sections 5.2 and 5.3, the steady-state analysis and operating principles are presented, respectively. The testing results for the 40 W prototype are presented in Chapter 6, and conclusions are provided in Section Chapter 7.

5.2 Proposed Led Driver and Operating Principles

The suggested LED driver's circuit structure is shown in (Fig. 3.1). A nonisolated LCLC resonant network composed of L_{r1}, C_{r1}, L_{r2}, and C_{r2}C that may offer CC functionality serves as the converter's fundamental component. The inverter switches S1 and S2 operate with a constant duty cycle of 0.5 and a switching frequency (f_s) equal to the resonant frequency (f_r). C_{s1}, C_{s2}, and C_{sa} are the total of the MOSFET output capacitances and the used snubber capacitors, and they supply the ZVS turn-OFF condition. The active voltage doubler rectifier, which controls the output current based on the Sa duty cycle, is made up of S_a and D_0. In this configuration, C_0 is the output capacitor and V_S is either the dc capacitor voltage of a traditional full-wave rectifier or the dc bus voltage supplied by a buck-boost-based PFC stage.

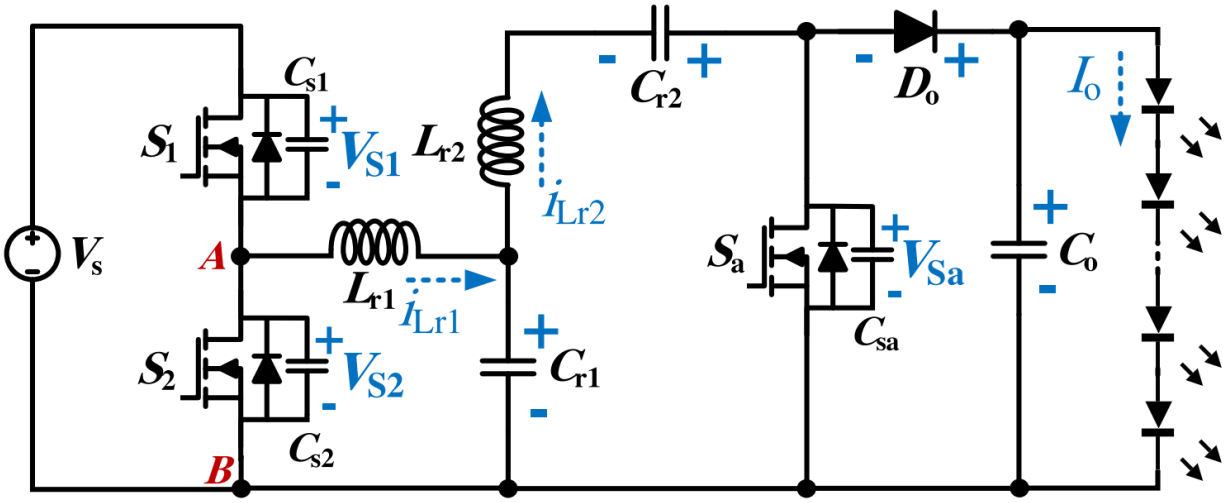

Fig. 3.1. Proposed LED driver circuit diagram

To simplify the converter's functioning, all components are assumed to be flawless, and the converter operates at steady state. Furthermore, it is anticipated that the output capacitor will be large enough to support the idea of the output voltage being constant during a switching cycle. Fig. 3.3 displays the key waveforms of the suggested converter. The operating modes may be divided into nine periods, and the corresponding converter circuit for each period is shown in Fig. 3.2.

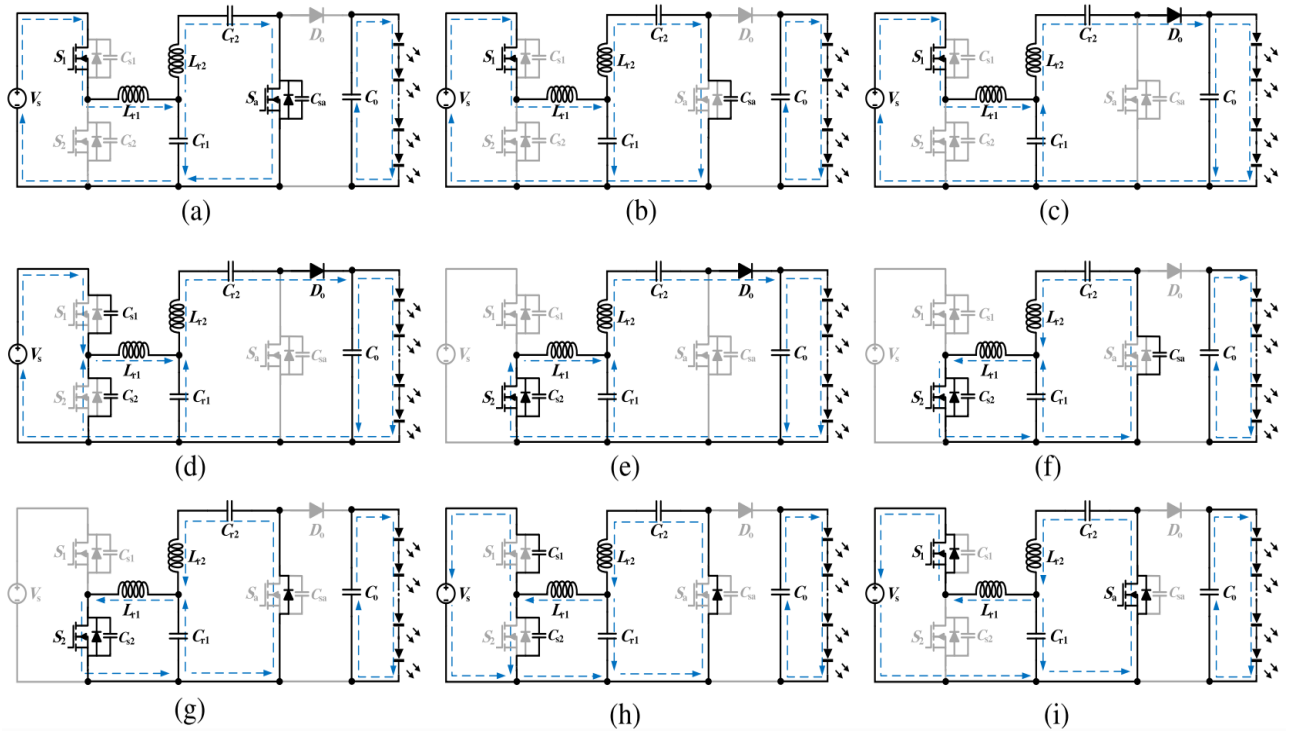

Fig. 3.2 Equivalent circuit of each operating interval.

(a) Interval 1. (b) Interval 2. (c) Interval 3. (d) Interval 4. (e) Interval 5.

(f) Interval 6. (g) Interval 7. (h) Interval 8. (i) Interval 9.

Interval 1 [t0–t1]:

In this interval, S1 and Sa are conducting, and D_0 is reversed biased. A resonant network containing L_{r1} , C_{r1} , L_{r2} *and* C_{r2} is formed. V_s is applied to the resonant network and I_{Lr1} increases in a sinusoidal manner. Also, Co supplies the load, and at t1, S_a is turned OFF at ZVS conditions.

Interval 2 [t1–t2]:

By turning S_a OFF, L_{r2} current charges C_{sa} in a resonant manner, and V_{sa} increases. At t2, V_{Sa} reaches V_0, which causes D_0 to conduct.

Interval 3 [t2–t3]:

During this interval, Do and S1 are conducting while C_{r2} and C_{r1} are being discharged by I_{Lr2}. At t3, S_1 is turned OFF and this mode ends.

Interval 4 [t3–t4]:

By turning S1 OFF, I_{Lr1} charges and discharges C_{s1} and C_{s2}, respectively, until at t4, and C_{s2} is completely discharged and D_{s2} turns ON. Hence, S_2 can be turned ON under ZVS condition.

Interval 5 [t4–t5]:

In this interval, S2 and D_0 are conducting. V_{Cr1} is placed across L_{r1}, and thus, L_{r1} discharges in a sinusoidal manner. At t5, I_{lr2} reaches zero and Do turns OFF under zero current switching (ZCS) conditions.

Interval 6 [t5–t6]:

During this interval, the resonance continues and, C_{sa} discharges through a resonance with L_{r2} until at t6, V_{sa} reaches zero and Sa body diode turns ON.

Interval 7 [t6–t7]:

In this interval, Sa body diode is conducting, C_{r1} and C_{r2} are being discharged and charged via I_{Lr1} and I_{Lr2}, respectively, while Co provides power to the load. At t7, S2 is turned OFF under ZVS condition and this mode ends.

Interval 8 [t7–t8]:

By turning S2 off, I_{Lr1} charges and discharges C_{s2} and C_{s1}, respectively. At t8, C_{s1} is completely discharged and S1 body diode turns ON.

Interval 9 [t8–t9]:

At the beginning of this interval, S1 and Sa are turned ON under ZVS condition, Vs is applied to the resonant network, and I_{Lr1} increases in a resonant manner. At t9, I_{Lr1} becomes positive and the next switching cycle starts.

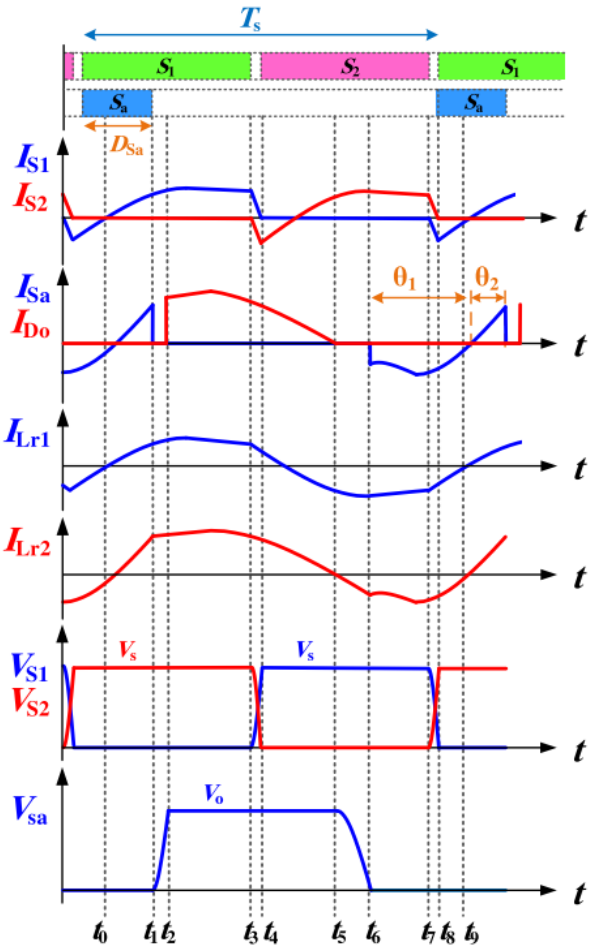

Fig. 3.3. Key waveforms of the proposed LED driver

5.3 Steady-State Analysis and Design Consideration

To achieve CC functioning, the suggested converter runs close to the resonant frequency. As a result, the majority of the power provided to the load is in the fundamental harmonic form, allowing the fundamental harmonic approximation (FHA) technique to be used for the theoretical analysis with sufficient accuracy [24]. The following parameters are defined before the analysis:

$$V_{AB,FHA}(t) = \frac{2V_s}{\pi}\cos(2\pi f_s t) \tag{21}$$

$$\omega_r = \frac{1}{\sqrt{L_{r1}C_{r1}}}, Z_r = \sqrt{\frac{L_{r1}}{C_{r1}}} \tag{22}$$

$$Q_e = \frac{Z_r}{R_{eq}} \tag{23}$$

$$L_n = \frac{L_{r2}}{L_{r1}}, C_n = \frac{C_{r2}}{C_{r1}} \tag{24}$$

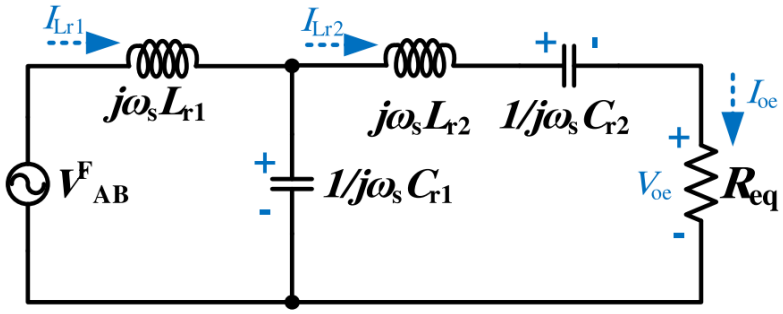

Fig. 3.4. FHA-equivalent circuit of the resonant network

5.3.1 Conversion Ratio

In Fig. 4, the LCLC network model in the frequency domain is presented, regarding the equivalent circuit, the voltage and current conversion ratios, M($j_{\omega n}$) and H($j_{\omega n}$), are as (25) and (26) shown below.

$$M(j\omega_n) = \frac{V_{oe}}{V_{AB,FHA}}$$

$$= \frac{j\omega_n C_n}{Q_e(1-\omega_n^2(1+L_n+C_n+L_nC_n+\omega_n^2 L_nC_n))+j\omega_n C_n(1-\omega_n^2)} \tag{25}$$

$$H(j\omega_n) = \frac{I_{oe}}{\left(\frac{V_{AB,FHA}}{Z_r}\right)}$$

$$= \frac{jC_n\omega_n}{1-\omega_n^2(1+C_n+L_nC_n(1-\omega_n^2))+j\omega_n\frac{C_n}{Q_e}(1-\omega_n^2)} \tag{26}$$

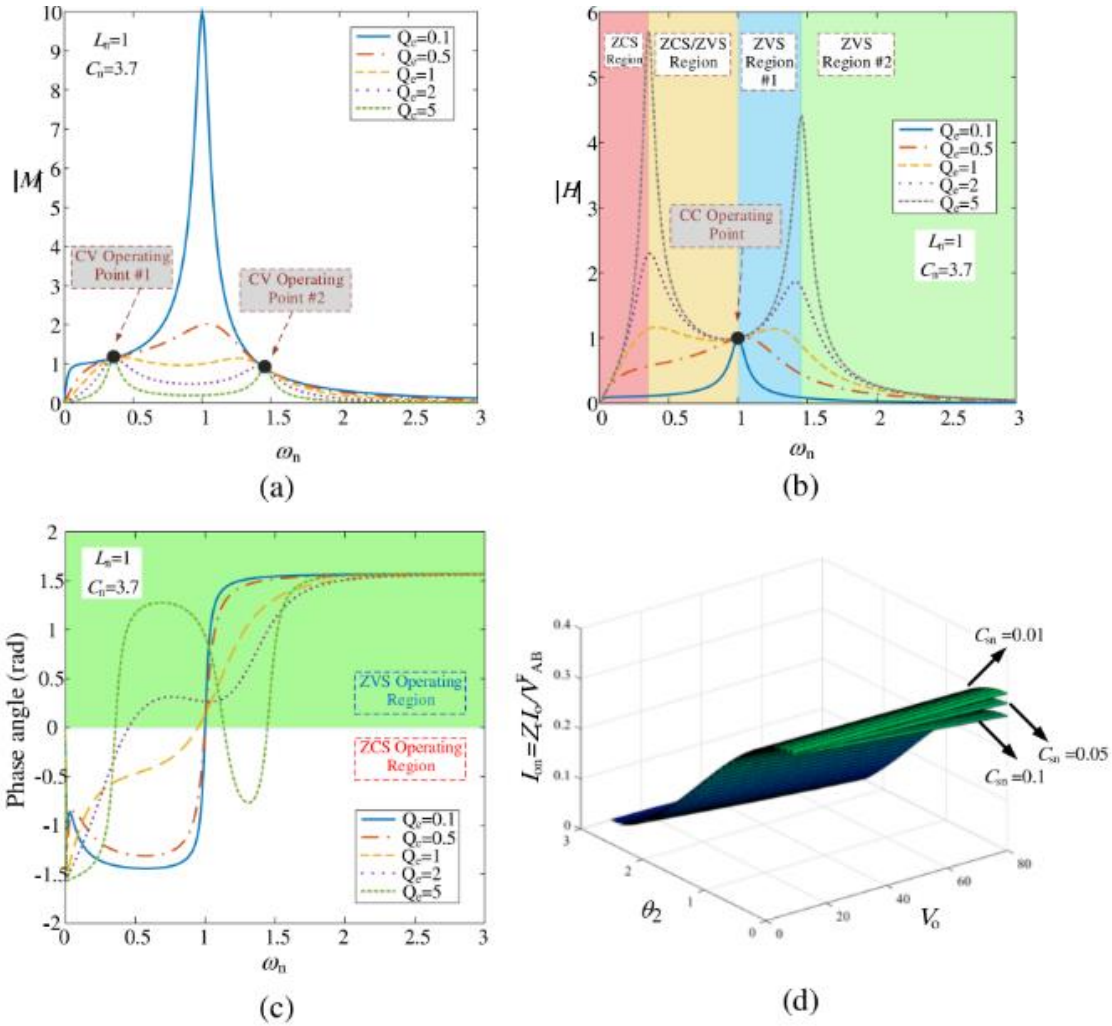

Fig. 3.5. (a) Voltage gain of LCLC resonant network. (b) Current gain of LCLC resonant network. (c) Input impedance phase angle of LCLC resonant network. (d) Normalized output current as a function of Sa conduction angle and output voltage

In Fig. 3.5(a) and (b), the magnitude graph of (25) and (26) for different values of Q_e is illustrated. As indicated, a load-independent output current characteristic can be realized in the vicinity of ω_n = 1. In this topology, the S_a duty cycle is adopted for adjusting the conversion ratio and the inverter switches operate at the constant duty cycle of 0.5. Since the average current of I_{D0} is delivered to the LED string, the I_0 value can be calculated using the FHA method, and considering the converter operation at the resonant frequency

$$I_0 = \begin{cases} \frac{V_S}{\pi^2 Z_r}(cos\theta_2 - cos\theta_2) & if\ \theta_2 < \theta_1 \\ 0 & if\ \theta_2 \geq \theta_1 \end{cases} \quad (27)$$

where, according to Fig. 3.3, θ_1 is the S_a body diode conduction angle, whereas θ_2 is the switch S_a conduction angle that can be calculated based on the S_a duty cycle as follows:

$$\theta_1 = 2cos^{-1}\sqrt{\frac{\pi C_{sn} V_0}{4V_s}} \tag{28}$$

$$\theta_2 = \begin{cases} 2\pi D_{sa} - \frac{\pi}{2} & if \ D_{sa} > \frac{1}{4} \\ 0 & if \ D_{sa} \leq \frac{1}{4} \end{cases} \tag{29}$$

$$C_{sn} = \frac{C_{sa}}{C_{r1}} \tag{30}$$

The output rectifying stage equivalent resistance (R_{eq}) is calculated as follows:

$$R_{eq} = \frac{V_0}{V_s} Z_r \sin\left(\frac{\theta_1 + \theta_2}{2}\right) \tag{31}$$

The input impedance phase angle of the LCLC resonant network for different values of Q_e is illustrated in Fig. 3.5(c). As observed, in the vicinity of the resonant frequency, by proper the selection of L_n and C_n, the ZVS turn-ON condition of the inverter switches can be improved for quality factors greater than one. Based on (7), the normalized graph of the output current (I_{0n}) versus θ_2 and V_0 for different values of C_{sn} is presented in Fig. 3.5(d). As illustrated, the output current can be controlled from maximum to zero by adjusting the S_a duty cycle, and C_{sn} has a small impact on the output current and the load-independent characteristic. Therefore, selecting small values of C_{sn} enhances the proposed converter performance.

5.3.2 Voltage and Current Stresses

According to the operating modes, the inverter switches voltage stress is limited to V_s. Also, S_a and D_0 voltage stress is limited to V_0 depending on the number of LEDs in a string. The rms current of S1 and S2 depends on the amplitude of I_{Lr1}, which can be expressed as follows:

$$I_{Lr1} = \frac{2V_s}{\pi Z_r}\left(\frac{1}{Q_e} - j\frac{1 + C_n(1 - L_n)}{C_n}\right) \tag{32}$$

Also, the rms current of S_a and D_0 depends on the amplitude of I_{Lr2}, which can be expressed as follows:

$$I_{Lr2} = -j\frac{2V_s}{\pi Z_r} \tag{33}$$

According to (36), the values of L_n and C_n impact the imaginary part of I_{Lr1}. As a result, the inverter switches rms current can be minimized for large values of C_n and L_n=1. However, regarding (37), the rms current of S_a and D_0 is independent of L_n and C_n. The inverter switches average current is equal to the input average current as follows:

$$\langle I_{S1} \rangle = \langle I_{S2} \rangle = \frac{P_0}{\eta V_s} \tag{34}$$

where P_0 is the output power, and η is the converter efficiency. Also, the average current of S_a and D_0 is equal to the output current.

5.3.3 ZVS Conditions

As stated in the converter steady-state analysis, the switching frequency of the inverter switches is chosen near the LCLC network resonant frequency to obtain CC characteristic. The snubber capacitors are considered for the main and auxiliary switches to achieve ZVS turn-OFF condition. The value of snubber capacitors can be obtained similar to [25] as follows:

$$C_s \geq C_{s_{min}} = \frac{i_{sw} t_f}{2 v_{sw}} \tag{35}$$

where i_{sw} is the switch current value before the turn-OFF instant, t_f is the switch current fall time, and v_{sw} is the switch voltage value at t_f . For providing the inverter switches ZVS turn-ON condition within the entire operating range, the Lr1 energy at the beginning of Intervals 4 and 8 should be large enough to provide complete discharge and charge of C_{s1} and C_{s2}, respectively. The inverter switches ZVS turn-ON criteria can be expressed as follows:

$$C_s V_s^2 < \frac{1}{2} L_{r1} I_{Lr1}^2(t_3) \tag{36}$$

Where $C_{s1} = C_{s2} = C_s$, and

$$I_{Lr1}(t_3) = \frac{2V_s}{\pi Z_r} \sqrt{\frac{1}{Q_e^2} + \frac{\left(1+C_n(1-L_n)\right)^2}{C_n^2}} \sin\left(2\pi f_s t_3 - \varphi\right) \tag{37}$$

$$\varphi = tan^{-1}\left(Q_e \frac{1+C_n(1-L_n)}{C_n}\right) \tag{38}$$

Equation (42) must be satisfied for the entire input voltage and output voltage ranges to guarantee the ZVS turn-ON condition of S1 and S2. For providing ZVS turn-OFF condition for S_a, a snubber capacitor should be employed. However, according to (31), the value of C_{sa} should be much smaller than C_{r1} to realize a proper CC operation for the LED string. The ZVS turn-ON condition of S_a is similar to the inverter switches, and the I_{Lr2} energy should satisfy the following criteria:

$$C_{sa} V_0^2 = L_{r2} I_{Lr2}^2(t_5) \tag{39}$$

$$I_{Lr2}(t_5) = \frac{2V_s}{\pi Z_r} \sin\left(2\pi f_s t_5 + \pi\right) \tag{40}$$

According to (43), at the worst-case condition of maximum V_0 and minimum V_s, I_{Lr2} amplitude at t5 should be large enough to guarantee the ZVS turn-ON condition for S_a.

5.3.4 Dimming and Open-Load Protection

Two dimming techniques can be used in the proposed LED driver by using the auxiliary switch. By adjusting the S_a duty cycle, analog dimming may be supplied for LEDs, as shown in Fig. 3.5(d). Additionally, the Sa gate signal can be modulated using the traditional PWM dimming technique utilizing a low-frequency PWM dimming signal. When the dimming signal is turned off in this approach, S_a continues to function normally and a steady current is given to the LED string. S_a conducts continuously and C_0 is quickly discharged through the LED string when the dimming signal is applied. C_0 is designed with a dimming frequency comparable to [18] in order to achieve an efficient PWM dimming. Be aware that an LC filter can be used in place of the output capacitor to decrease size [21]. The suggested topology also has a CC feature, which means that the converter may be harmed if the LED string were to suddenly detach. Sa may also provide open-load safety by turning ON continuously if the LED string is detected to be disconnected since it is connected in parallel with the load.

Chapter 6

Experimental Validation

In this section, the proposed topology is designed for supplying a 40-W LED string involving 243.3 V high-brightness (HB) white LEDs. Then, the prototype circuit experimental results are presented. Finally, the proposed driver is compared with the state-of-the-art LED drivers

6.1 Design Procedure

The values of $Lr1, Lr2, Cr1, and\ Cr2$ are determined in order to construct the suggested converter for the particular input voltage and load circumstances. For the purpose of developing the suggested converter, it is assumed that the input voltage is provided by either the typical full-wave rectifier output capacitor with a grid voltage range of 85 to 130 Vrms or the dc-link of a buck-boost-based PFC stage. The recommended converter input voltage can be within the range of 80–230 V, and the maximum voltage ripple of 40 V is taken into account in order to limit the size of the dc-link capacitor. At the output stage, 24 series HB-LEDs with typical characteristics of 3.3 V500 mA are used, resulting in an output voltage of 80 V.

The suggested converter is intended to deliver the nominal output current at the minimal auxiliary switch conduction angle at a minimum input voltage of 80 V. By modifying the Sa duty cycle, the output current may be controlled at 500 mA at higher input voltages. In order to provide the maximum output current of 520 mA at 80 V input voltage, Zr = 29.4 is computed based on (7) and the assumption that $\theta 2 = 0$, Calculations may be made to determine the values of Lr1 and Cr1 for a 200 kHz switching frequency.

$$L_{r1} = \frac{Z_r}{2\pi f_s} = 23.5\ \mu H \tag{41}$$

$$C_{r1} = \frac{Z_r}{2\pi f_s Z_r} = 27\ nF \tag{42}$$

Based on (36), L_{r1} = L_{r2} = 23.5 μH is chosen to lower the inverter switches' rms currents. Additionally, C_{s1} and C_{s2} are set to 1 nF in order to provide ZVS turn-OFF conditions for the inverter switches. Then, according to (16), the proper value of C_{r2} = 100 nF is selected for realizing ZVS turn-ON condition for S1 and S2. Selecting the proper value of C_{sa} requires a

trade-off, and according to (31), the value of C_{sa} should be selected much smaller than C_{r1} for retaining the strong CC operation. As a result, to provide the ZVS turn-OFF condition for Sa without diminishing the CC characteristic, the proper value of C_{sa} is chosen 1 nF.

Table: I

Parameters of Implemented Prototype

Parameter/Component	Symbol	Specification
DC input voltage range	V_s	80-230 V
Nominal Output power	P_0	40 W
Switching Frequency	f_s	200 kHz
Resonant inductors	L_{r1} , L_{r2}	23.5 μH
First resonant capacitor	C_{r1}	27 nF
Second resonant capacitor	C_{r2}	100 nF
Snubber capacitor	C_{s1} , C_{s2} , C_{sa}	1 nF
Output Capacitor	C_0	4.7 μH
Nominal output Current	I_0	500 mA

6.2 Test Setup and Methodology

To validate the performance and feasibility of the proposed High-Performance Parallel Resonant Converter (HPPRC) for LED driver applications, a comprehensive test setup and methodology were devised. This section outlines the experimental setup, measurement instruments, and procedures utilized to assess the behaviour of the HPPRC under various conditions.

6.2.1 Experimental Setup

The HPPRC circuit was implemented according to the designed specifications, including the resonant tank circuit, switching components, and control circuitry using PSIM.

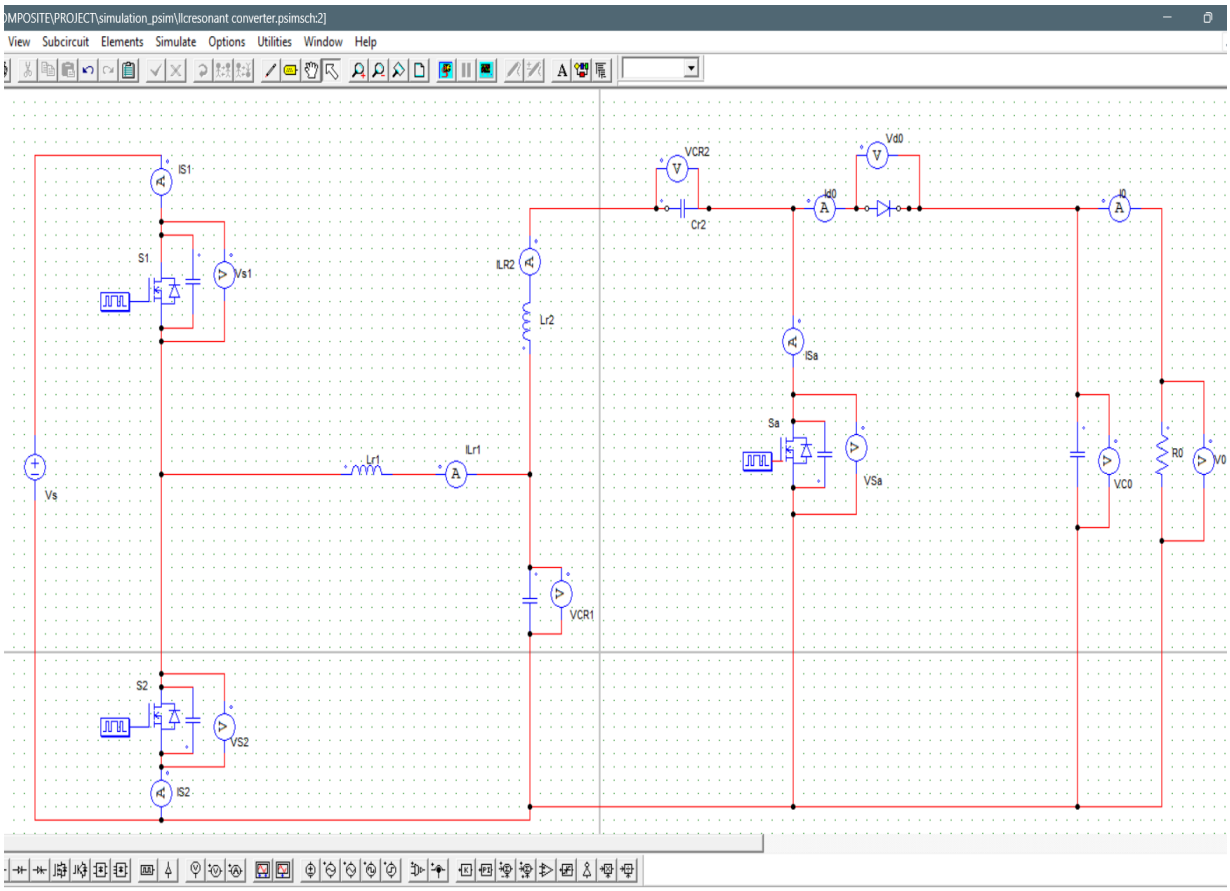

Fig. 4.1 Proposed converter simulation circuit.

6.2.2 Simulation and result

In order to gain comprehensive insights into the behaviour and performance of the proposed High-Performance Parallel Resonant Converter (HPPRC) for LED driver applications, a rigorous simulation study was conducted. This section details the simulation methodology, presents the simulated results, and discusses the implications of these findings.

6.2.2.1 Simulation Methodology

The simulation study was carried out using ***PSIM***, a powerful tool known for its ability to accurately model complex power electronic circuits. The proposed HPPRC circuit was accurately replicated in the simulation environment, including the resonant tank, switching components, control circuits, and LED load.

6.2.2.2 Simulated Results and Analysis

The experimental implementation and testing of the proposed LED driver, present a comprehensive evaluation of the High-Performance Parallel Resonant Converter (HPPRC) for LED driver applications. The meticulous examination of the converter's behaviour under diverse operational conditions, as evidenced by the reported experimental results and accompanying waveforms, yields invaluable insights into its feasibility, robustness, and performance.

The realization of the simulated prototype(200-kHz) of the HPPRC stands as a significant accomplishment, representing the culmination of the theoretical framework's translation into a tangible device. The alignment of the prototype's specifications with those summarized in Table I showcases a meticulous design process that adheres to predetermined requirements, reflecting a systematic approach to converter development.

The semiconductor devices' experimental waveforms, shown in Figs. 4.2 and 4.3, demonstrate the inverter switches' attainment of Zero-Voltage Switching (ZVS) throughout the full input voltage range. The ZVS functioning underlines the resonant converter's practical viability in addition to validating its theoretical assumption. Additionally, the stringent restriction of voltage stress on devices like S1, S2, and Sa to the input or output voltage supports efficient control schemes and safeguards against device failure brought on by high stress levels. Additionally, the experimental waveforms of ILr1, ILr2, VCr1, and VCr2 at input voltages of 80 and 230 V are presented in Figures 4.4 and 4.5.

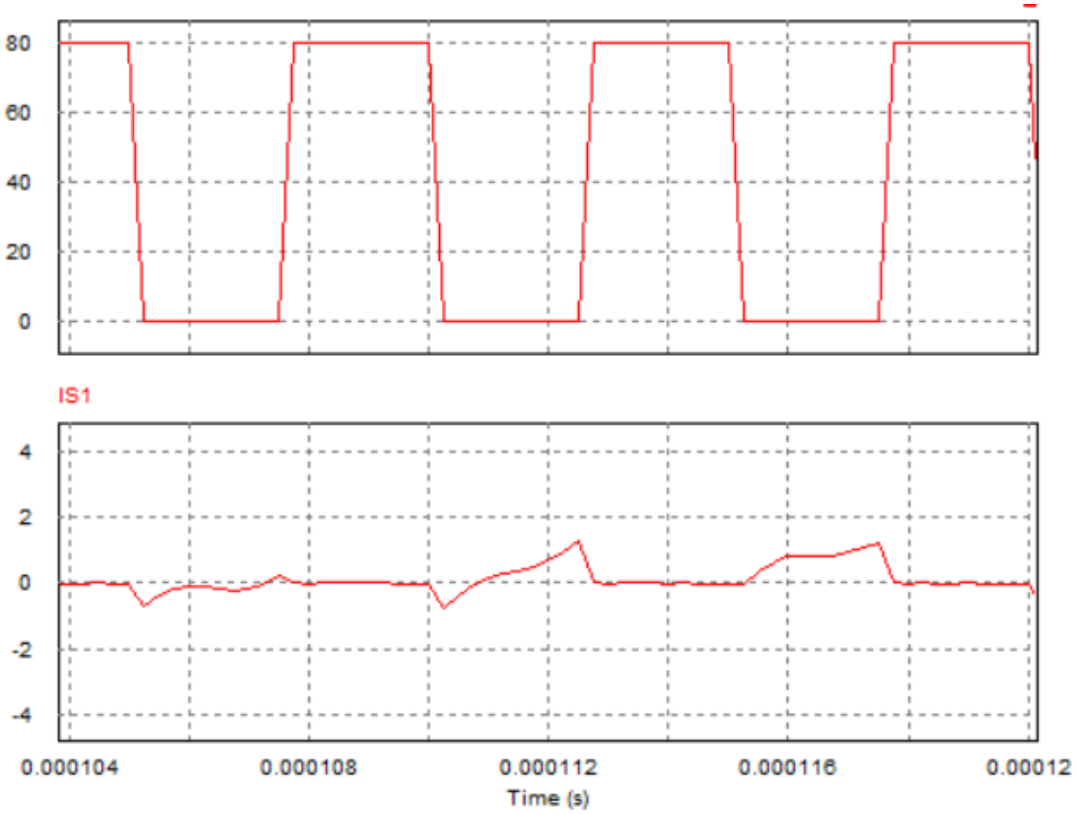
80
60
40
20
0
IS1
4
2
0
-2
-4
0.000104
0.000108
0.000112
0.000116
0.00012
Time (s)

(a)

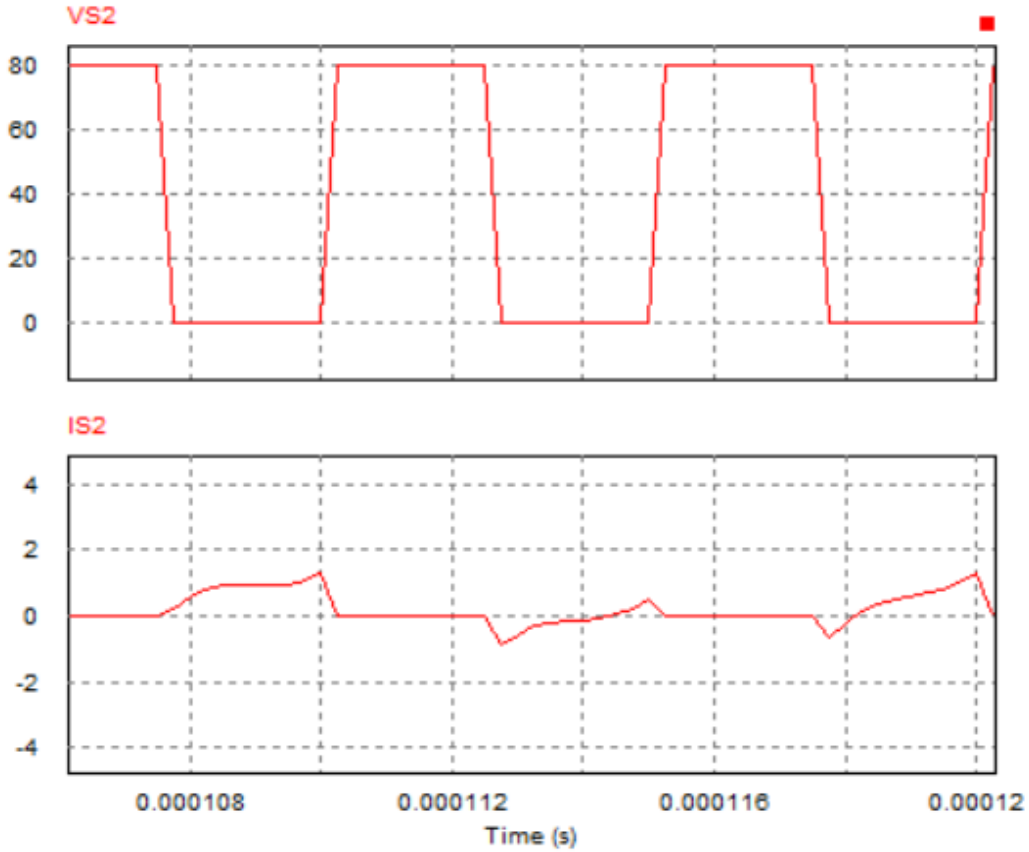
VS2
80
60
40
20
0
IS2
4
2
0
-2
-4
0.000108
0.000112
0.000116
0.00012
Time (s)

(b)

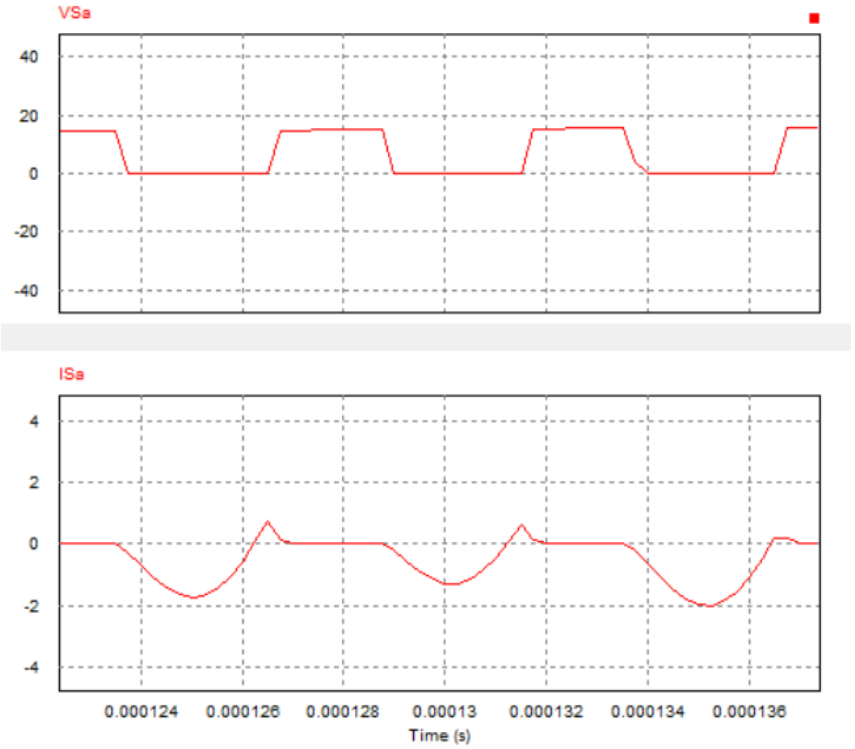

(C)

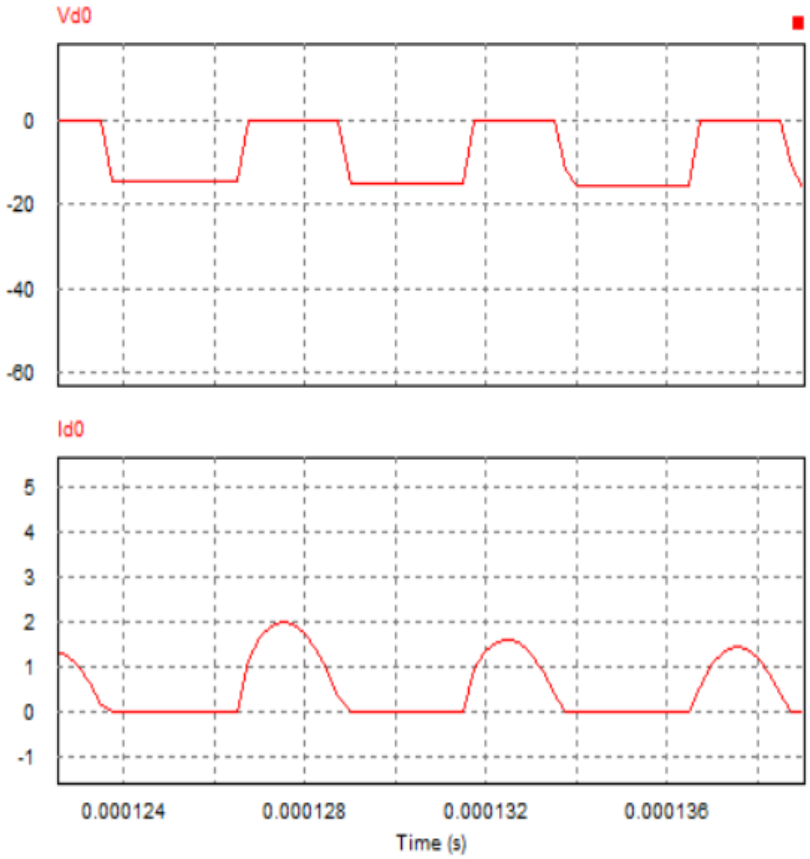

(d)

Fig. 4.2. Simulated waveforms semiconductor devices at 80 V input voltage. (a) S1. (b) S2. (c) Sa. (d) Do.

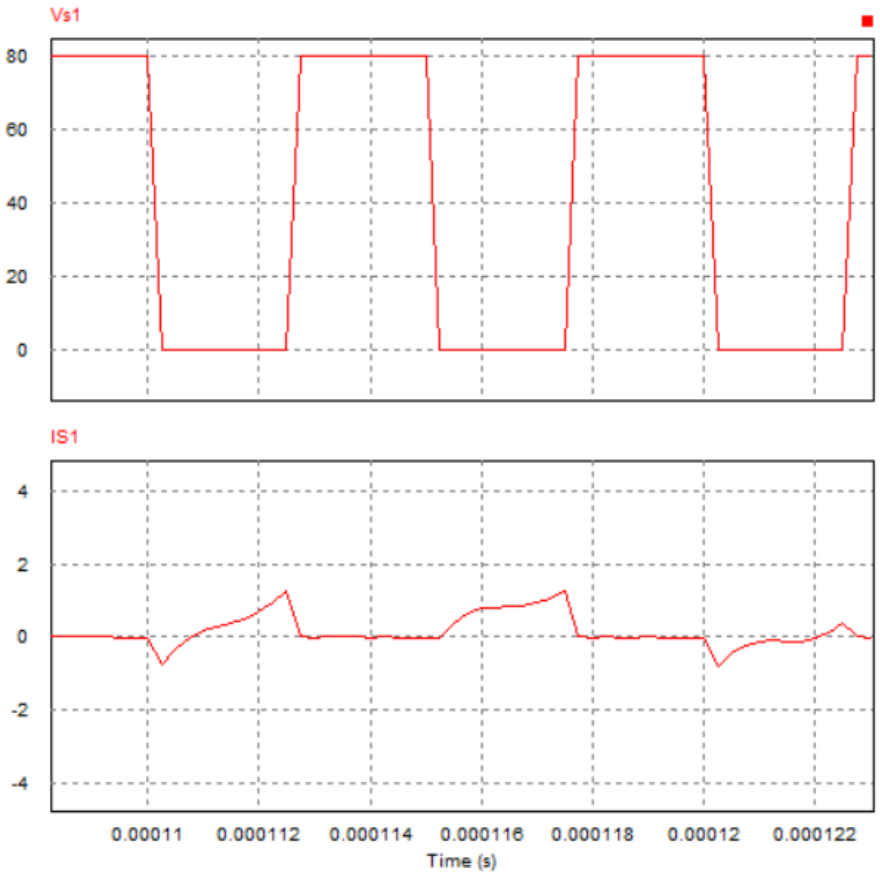
Vs1
80
60
40
20
0
IS1
4
2
0
-2
-4
0.00011
0.000112
0.000114
0.000116
0.000118
0.00012
0.000122
Time (s)

(a)

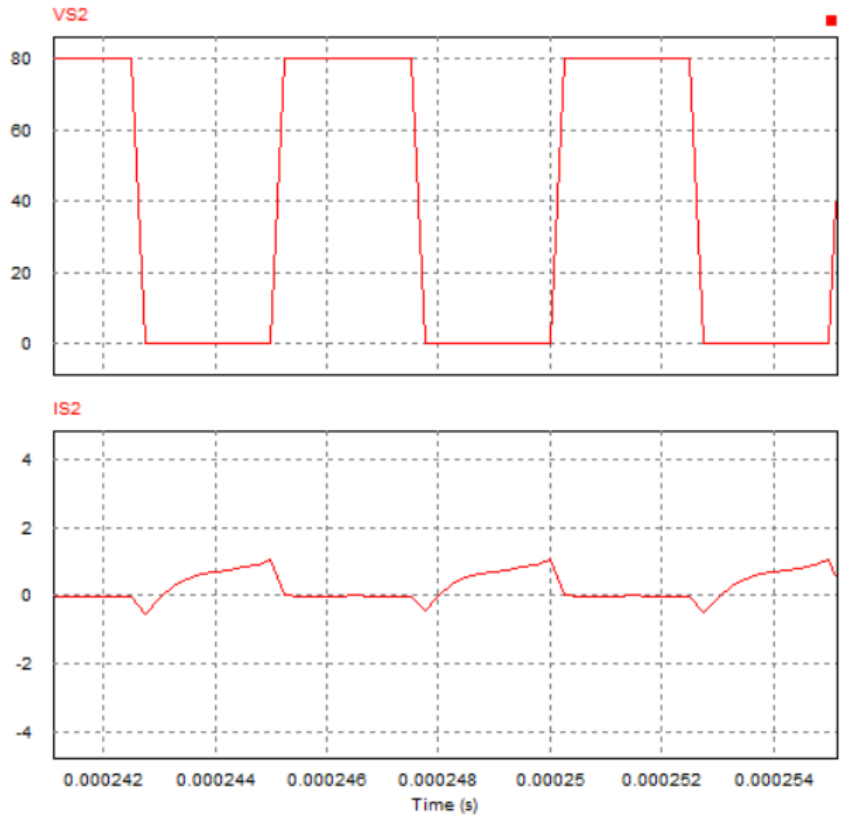
VS2
80
60
40
20
0
IS2
4
2
0
-2
-4
0.000242
0.000244
0.000246
0.000248
0.00025
0.000252
0.000254
Time (s)

(b)

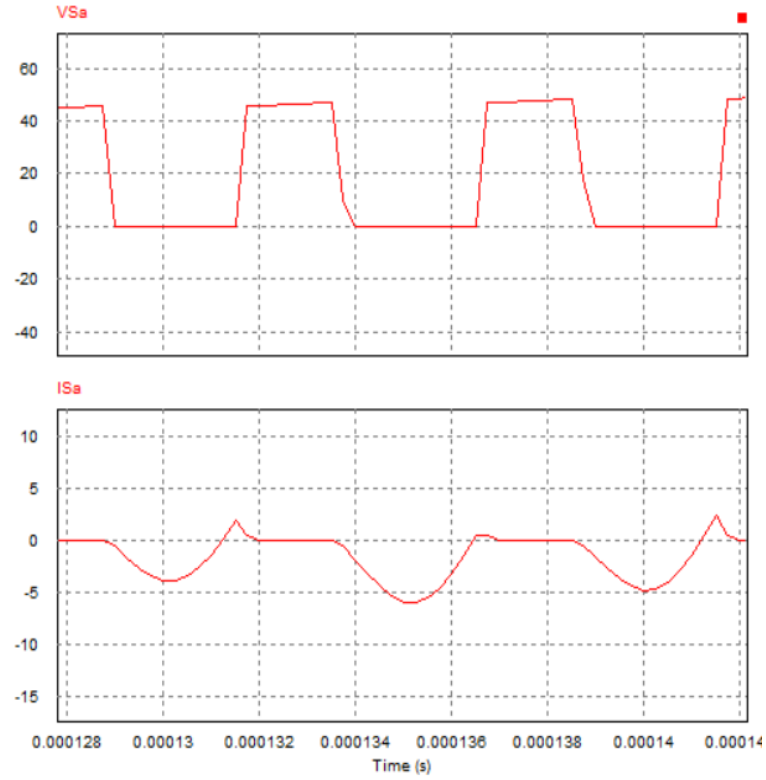

(c)

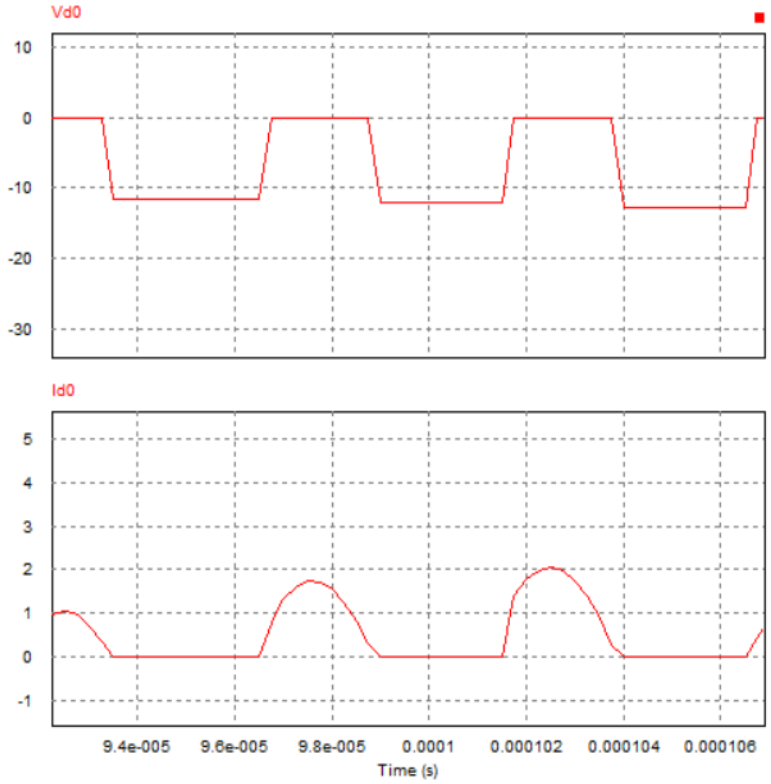

(d)

Fig. 4.3. Simulated waveforms semiconductor devices at 230 V input voltage. (a) S1. (b) S2. (c) Sa. (d) Do.

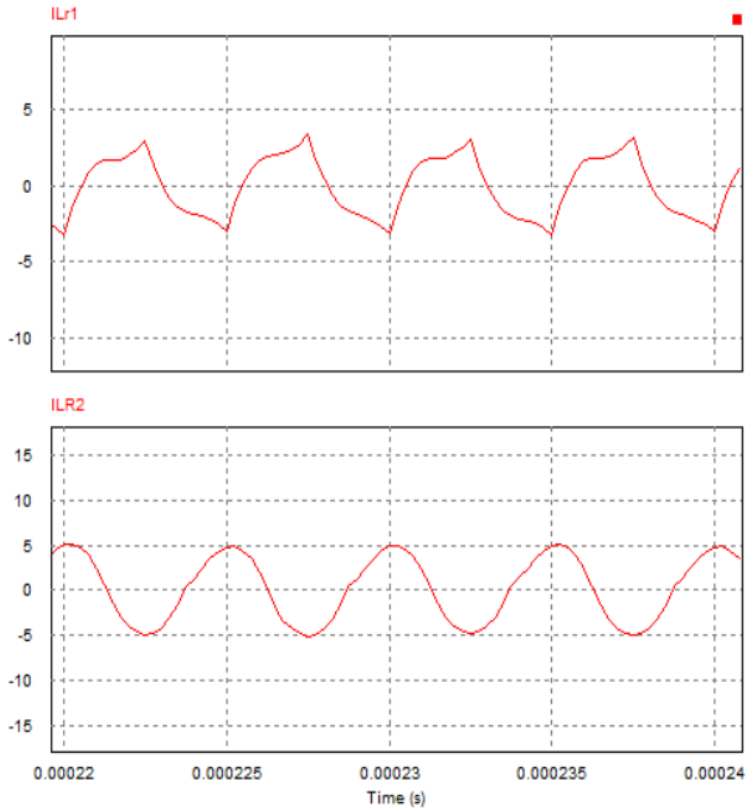

(a)

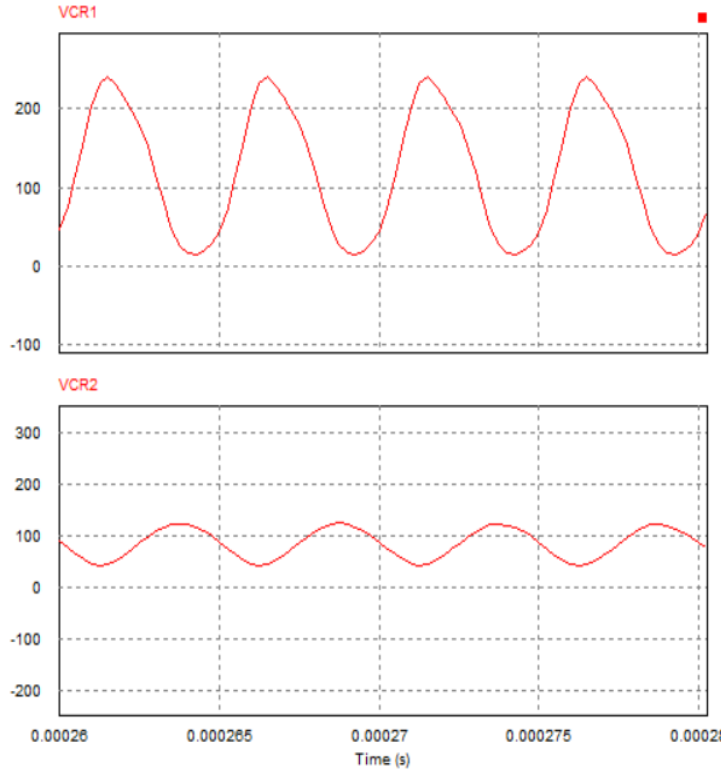

(b)

Fig. 4.4. Simulated waveforms of resonant components at different input voltages. (a) ILr1 and ILr2 at 80 V. (b) VCr1 and VCr2 at 240 V

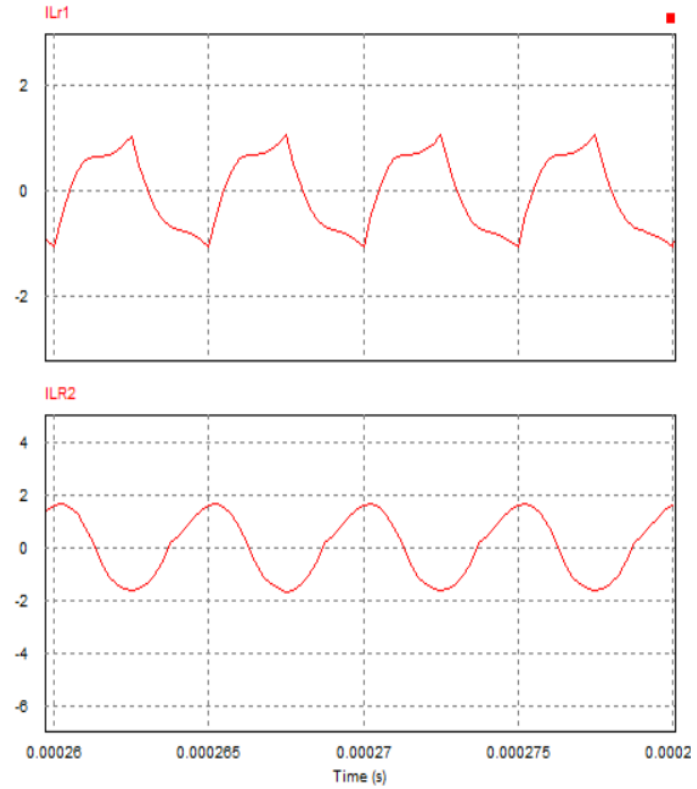

(a)

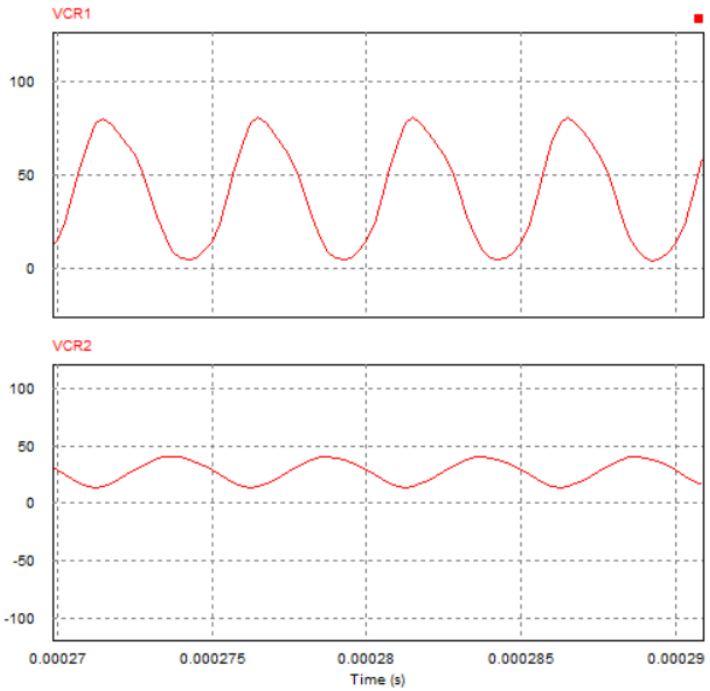

(b)

Fig. 4.5. Simulated waveforms of resonant components at different input voltages. (a) ILr1 and ILr2 at 80 V. (b) VCr1 and VCr2 at 80 V

6.3 Comparison

The exploration of the High-Performance Parallel Resonant Converter (HPPRC) and its implications for LED driver applications yields valuable insights that contribute to the advancement of power conversion technologies in the realm of lighting systems. This section delves into the interpretation of the obtained results, a comparison with existing solutions, the implications of the proposed converter for LED driver applications, as well as its limitations and future research directions.

6.3.1 Interpretation of Results

The interpretation of the experimental and simulated results sheds light on the behaviour, characteristics, and performance of the proposed High-Performance Parallel Resonant Converter (HPPRC). The realization of ZVS and ZCS operations, as validated by the experimental waveforms, affirms the converter's resonance-based design and its potential for reduced switching losses. The consistent voltage stress management of the semiconductor devices highlights the efficacy of control strategies in maintaining device reliability. Furthermore, the transient response waveforms underscore the converter's stability during dynamic load changes and its capacity for prompt open-load protection.

The efficiency diagram demonstrates the remarkable energy-efficient performance of the HPPRC, with an average efficiency of around 97% at full load across various input voltages. The peak efficiency of 97.8% at an 80V input voltage attests to the converter's effectiveness even under challenging conditions. The loss analysis corroborates the efficiency observations and guides potential areas for improvement in future design iterations.

6.3.2 Comparison with Existing Solutions

A comparison between the proposed converter and recently reported resonant converters for LED driver applications in terms of component count, semiconductor voltage stress, soft switching operation, reported input voltage and output voltage ranges, control method, and reported full-load efficiency is summarized in Table II. According to this comparison, the proposed converter enjoys PWM operation using an auxiliary switch and inherent CC feature. As a result, it can properly operate with wide variations of the input and output voltage.

In comparison to existing solutions, the High-Performance Parallel Resonant Converter (HPPRC) offers distinct advantages that make it a promising candidate for LED driver applications. Unlike conventional non-resonant converters, the HPPRC capitalizes on resonant tank operation to reduce switching losses and enhance efficiency. This advantage becomes particularly evident in the achieved ZVS and ZCS operations, showcasing the converter's potential to significantly minimize switching-related losses. Moreover, the converter's robust transient response and efficient open-load protection further set it apart from conventional solutions.

Table: II

Performance Comparison with State-Of-The-Art Resonant Led Drivers

Characteristics	*Proposed*	*[17]*	*[18]*	*[20]*	*[21]*	*[22]*	*[26]*
Number of Switches	3	4	5	4	6	8	1
Number of Switches	2	4	2	-	-	-	2
Number of Switches	2	2	2	2	3	3	2
Capacitors	3	3	3	4	3	6	3
Main Switches	Vs	Vs/(1-D)	Vs	Vs	Vs	DVs/1-D	3Vs
Output diodes/switches	Vo	Vo/2	Vo	Vo	Vo	Vo	Vs
Control Method	PWM	PWM	PWM	PSC	PSC	PWM	VFC
Reported input voltage range	80-240	18-120	48	14	8-18	8-18	130-190
Reported output voltage range	77-232	22.5	3.3-20	3.3-49.5	3-45	3-50	80
Reported full load efficiency	97	91.2	91.2	91	85	91	92
Nominal Power	40	22	30	25	20	50	40

This table demonstrates that the recommended architecture has fewer components and complete ZVS functionality when compared to [17], [18], [20], [21], and [22]. In contrast to [17], [18], and [22], the recommended converter also has a no cascaded structure, which offers more efficiency. The design described in [26] is built on the Class E resonant converter, which only requires one switch. However, due to the switch's voltage stress being substantially higher than its input voltage, variable frequency control is required to control the output current, which is inappropriate for applications requiring a broad range of input voltages due to frequency changes. Due to the phase-shift modulation approach employed in [20] and [21], which increases component count, complexity, and imposes extra circulation loss, higher losses arise when the converter operates over the wide input and output voltage ranges. In the two-stage converter depicted in [22], the output current is controlled by the front-end buck-boost stage duty cycle. But the cascaded design results in an increase in component count, hard switching during buck-boost stage operation, and reduced effectiveness.

Chapter 7

Conclusion

In conclusion, this research has introduced a nonisolated resonant LCLC converter tailored for LED driver applications. The adopted resonant network, characterized by constant current operation, emerges as an optimal fit for LED lighting systems. The converter's ability to deliver full soft switching performance across a wide range of input and output voltages, achieved with optimized rms current, underscores its efficiency and adaptability. By employing an auxiliary switch for regulating output current under varying input voltages, the converter not only addresses dynamic load variations but also facilitates PWM dimming and open-load protection for LEDs.

7.1 Summary of Contributions

This study presents significant contributions to the field of power electronics and LED driver technology:

Resonant LCLC Converter Design: The conceptualization and design of a nonisolated resonant LCLC converter catered specifically to LED driver applications showcase a unique approach to achieving efficient and soft-switching operation.

Constant Current Operation: The incorporation of constant current operation within the resonant network aligns the converter's behavior with the demands of LED lighting systems, ensuring consistent and stable illumination.

Auxiliary Switch Implementation: The integration of an auxiliary switch introduces dynamic control capabilities, enabling output current regulation, PWM dimming, and open-load protection.

Theoretical Framework: Theoretical analysis and the converter's design procedure, rooted in the FHA method, contribute to the understanding of its behavior and guide its practical realization.

7.2 Practical Relevance and Significance

The proposed converter's practical relevance and significance within LED driver applications are substantial. By addressing the challenges of efficient power conversion and reliable illumination in a single solution, the converter offers an innovative means to optimize LED lighting systems. Its ability to maintain high efficiency within a wide input voltage range ensures its adaptability to varying power supply conditions, enhancing its utility in diverse environments. The incorporation of auxiliary switch control further amplifies its value by providing essential features for modern LED applications, such as dimming and protection mechanisms.

7.3 Limitations and Future Research Directions

While the proposed High-Performance Parallel Resonant Converter (HPPRC) exhibits impressive characteristics, it is essential to acknowledge its limitations and chart future research directions. One of the key limitations is the reliance on precise component selection and sizing, which might present challenges in scenarios with component variability. Future research could focus on developing control strategies that accommodate component tolerances and variations without compromising performance.

Future research directions encompass a spectrum of opportunities. Advanced control strategies, such as predictive and adaptive algorithms, offer potential for further enhancing efficiency and dynamic response. Exploring hybrid resonant topologies, integration with smart lighting systems, and multi-converter configurations could lead to more versatile and scalable solutions. Design optimization efforts could delve deeper into component selection, soft-switching techniques, and magnetic design considerations to fine-tune efficiency and power density. Additionally, research into reliability enhancement through advanced thermal management, fault tolerance mechanisms, and environmentally conscious design practices aligns with sustainability goals.

In summary, the interpretation of results showcases the HPPRC's efficient and robust behavior. A comparison with existing solutions highlights its innovative advantages. The implications for LED driver applications underscore its transformative potential. While acknowledging its limitations, future research directions promise to propel the HPPRC's performance and integration in the realm of modern lighting systems.

7.4 Concluding Remarks

This article has showcased the potential of the proposed nonisolated resonant LCLC converter through a comprehensive theoretical analysis, design methodology, and experimental validation. The realization of a 200 kHz prototype, capable of delivering a steady 0.5 A current to a string of 24 series HB-LEDs, underscores the converter's feasibility and practicality. Achieving an impressive average full load efficiency of 97% across a wide input voltage range (80–230 V) reinforces its potential for energy-efficient LED driver applications.

As the world progresses towards energy-efficient and sustainable lighting solutions, the contributions of this research find resonance. The presented converter not only exemplifies technological innovation but also holds promise for shaping the future of LED driver systems, by offering enhanced efficiency, dynamic control capabilities, and reliability across diverse operating conditions.

REFERENCES

[1] Y. Wang, J. M. Alonso, and X. Ruan, “A review of LED drivers and related technologies,” IEEE Trans. Ind. Electron., vol. 64, no. 7, pp. 5754–5765, Jul. 2017.

[2] F. Pouladi, H. Farzanehfard, E. Adib, and H. Le Sage, “Single-switch soft-switching LED driver suitable for battery-operated systems,” IEEE Trans. Ind. Electron., vol. 66, no. 4, pp. 2726–2734, Apr. 2019.

[3] M. Borage, S. Tiwari, and S. Kotaiah, “LCL-T resonant converter with clamp diodes: A novel constant-current power supply with inherent constant-voltage limit,” IEEE Trans. Ind. Electron., vol. 54, no. 2, pp. 741–746, Apr. 2007.

[4] J. Zhao et al., “Fast and accurate control strategy for LCC resonant converters based on simplified state trajectory and two-point solution method,” IEEE Trans. Power Electron., vol. 37, no. 5, pp. 5309–5319, May 2022.

[5] N. Shafiei, M. Ordonez, M. A. Saket Tokaldani, and S. A. Arefifar, “PV battery charger using an L3C resonant converter for electric vehicle applications,” IEEE Trans. Trans. Elect., vol. 4, no. 1, pp. 108–121, Mar. 2018.

[6] H.-N. Vu and W. Choi, “A novel dual full-bridge LLC resonant converter for CC and CV charges of batteries for electric vehicles,” IEEE Trans. Ind. Electron., vol. 65, no. 3, pp. 2212–2225, Mar. 2018.

[7] J. A. Martın-Ramos, P. J. Villegas Sáiz, A. M. Pernıa, J. Dıaz, and J. A. Martınez, “Optimal control of a high-voltage power supply based on the PRC-LCC topology with a capacitor as output filter,” IEEE Trans. Ind. Appl., vol. 49, no. 5, pp. 2323–2329, Sep./Oct. 2013.

[8] A. Navarro-Crespin, R. Casanueva, and F. J. Azcondo, “Performance improvements in an ARC-welding power supply based on resonant inverters,” IEEE Trans. Ind. Appl., vol. 48, no. 3, pp. 888–894, May/Jun. 2012.

[9] M. F. Menke, J. P. Duranti, L. Roggia, F. E. Bisogno, R. V. Tambara, and R. Seidel, “Analysis and design of the LLC LED driver based on state-space representation direct time-domain solution,” IEEE Trans. Power Electron., vol. 35, no. 12, pp. 12686–12701, Dec. 2020.

[10] J.-W. Kim, J.-P. Moon, and G.-W. Moon, “Duty-ratio-control-aided LLC converter for current balancing of two-channel LED driver,” IEEE Trans. Ind. Electron., vol. 64, no. 2, pp. 1178–1184, Feb. 2017.

[11] H. Ma, Y. Li, Q. Chen, L. Zhang, and J. Xu, “A single-stage integrated boost-LLC AC–DC converter with quasi-constant bus voltage for multi-channel LED street-lighting applications,” IEEE Trans. Emerg. Sel. Topics Power Electron., vol. 6, no. 3, pp. 1143–1153, Sep. 2018.

[12] X. Tang, Y. Xing, H. Wu, and J. Zhao, “An improved LLC resonant converter with reconfigurable hybrid voltage multiplier and PWM-plus-PFM hybrid control for wide output range applications,” IEEE Trans. Power Electron., vol. 35, no. 1, pp. 185–197, Jan. 2020.

[13] C. Li, M. Zhou, and H. Wang, “An H5-bridge-based asymmetric LLC resonant converter with an ultrawide output voltage range,” IEEE Trans. Ind. Electron., vol. 67, no. 11, pp. 9503–9514, Nov. 2020.

[14] L. A. D. Ta, N. D. Dao, and D.-C. Lee, “High-efficiency hybrid LLC resonant converter for on-board chargers of plug-in electric vehicles,” IEEE Trans. Power Electron., vol. 35, no. 8, pp. 8324–8334, Aug. 2020.

[15] X. Chen, D. Huang, Q. Li, and F. C. Lee, “Multichannel LED driver with CLL resonant converter,” IEEE Trans. Emerg. Sel. Topics Power Electron., vol. 3, no. 3, pp. 589–598, Sep. 2015.

[16] Y. Wang, S. Gao, Y. Guan, J. Huang, D. Xu, and W. Wang, “A single-stage LED driver based on double LLC resonant tanks for automobile headlight with digital control,” IEEE Trans. Transp. Electrific., vol. 2, no. 3, pp. 357–368, Sep. 2016.

[17] V. K. S. Veeramallu, S. Porpandiselvi, and B. L. Narasimharaju, “A non-isolated wide input series resonant converter for automotive LED lighting system,” IEEE Trans. Power Electron., vol. 36, no. 5, pp. 5686–5699, May 2021.

[18] X. Qu, S.-C. Wong, and C. K. Tse, “An improved LCLC current-sourceoutput multistring led driver with capacitive current balancing,” IEEE Trans. Power Electron., vol. 30, no. 10, pp. 5783–5791, Oct. 2015.

[19] Y. Wang, X. Deng, Y. Wang, and D. Xu, “Single-stage bridgeless LED driver based on a CLCL resonant converter,” IEEE Trans. Ind. Appl., vol. 54, no. 2, pp. 1832–1841, Mar./Apr. 2018.

[20] M. Khatua et al., “High-performance megahertz-frequency resonant DC– DC converter for automotive LED driver applications,” IEEE Trans. Power Electron., vol. 35, no. 10, pp. 10396–10412, Oct. 2020.

[21] S. Mukherjee, V. Yousefzadeh, A. Sepahvand, M. Doshi, and D. Maksimovi´c, “High-frequency wide-range resonant converter operating as an automotive LED driver,” IEEE Trans. Emerg. Sel. Topics Power Electron., vol. 9, no. 5, pp. 5781–5794, Oct. 2021.

[22] S. Mukherjee, V. Yousefzadeh, A. Sepahvand, M. Doshi, and D. Maksimovi´c, “A two-stage automotive LED driver with multiple outputs,” IEEE Trans. Power Electron., vol. 36, no. 12, pp. 14175–14186, Dec. 2021.

[23] N. Molavi and H. Farzanehfard, “Load-independent hybrid resonant converter for automotive LED driver applications,” IEEE Trans. Power Electron., vol. 37, no. 7, pp. 8199–8206, Jul. 2022.

[24] M. Daryaei, M. Ebrahimi, and S. A. Khajehoddin, “Alternative approach to analysis and design of series resonant converter at steady state,” IEEE Trans. Ind. Electron., vol. 66, no. 6, pp. 4424–4435, Jun. 2019.

[25] R. W. Erickson and D. Maksimovic, Fundamentals of Power Electronics. New York, NY, USA: Springer, 2007.

[26] J. Ribas, P. J. Quintana-Barcia, J. Cardesin, A. J. Calleja, and E. L. Corominas, “LED series current regulator based on a modified class-e resonant inverter,” IEEE Trans. Ind. Electron., vol. 65, no. 12, pp. 9488–9497, Dec. 2018.

[27] Navid Molavi, Hosein Farzanehfard, “A Nonisolated Wide-Range Resonant Converter for LED Driver Applications,” IEEE Transactions on Industrial Electronics, Vol. 70, No. 9, September 2023.

[28] Hong Huang, “Designing an LLC Resonant Half-Bridge Power Converter,” Texas Instruments Power Supply Design Seminar SEM1900, Topic 3 TI Literature Number: SLUP263, 2010.